

JGR Earth Surface

L

RESEARCH ARTICLE

10.1029/2022JF007031

Key Points:

- Interferometric Synthetic Aperture Rader data on objects constructed on soft soil without a foundation are used for subsidence measurements
- Shrinkage of clay by aeration as a result of artificially lowered phreatic groundwater levels is identified as the main source of subsidence
- One meter drop in phreatic groundwater level now translates into 1 cm of subsidence in 5 years

Supporting Information:

Supporting Information may be found in the online version of this article.

Correspondence to:

M. Verberne, m.a.m.verberne@uu.nl

Citation:

Verberne, M., Koster, K., Lourens, A., Gunnink, J., Candela, T., & Fokker, P. A. (2023). Disentangling shallow subsidence sources by data assimilation in a reclaimed urbanized coastal plain, South Flevoland polder, the Netherlands. *Journal of Geophysical Research: Earth Surface*, 128, e2022JF007031. https://doi.org/10.1029/2022JF007031

Received 14 DEC 2022 Accepted 4 JUN 2023

Author Contributions:

Conceptualization: Manon Verberne, Kay Koster, Thibault Candela, Peter A. Fokker

Data curation: Manon Verberne, Aris Lourens, Jan Gunnink, Peter A. Fokker Formal analysis: Manon Verberne, Kay Koster

Funding acquisition: Kay Koster, Peter A. Fokker

Investigation: Manon Verberne, Peter A. Fokker

© 2023. The Authors.

This is an open access article under the terms of the Creative Commons Attribution-NonCommercial-NoDerivs License, which permits use and distribution in any medium, provided the original work is properly cited, the use is non-commercial and no modifications or adaptations are made.

Disentangling Shallow Subsidence Sources by Data Assimilation in a Reclaimed Urbanized Coastal Plain, South Flevoland Polder, the Netherlands

Manon Verberne^{1,2}, Kay Koster³, Aris Lourens³, Jan Gunnink³, Thibault Candela², and Peter A. Fokker^{1,2}

¹Faculty of Geosciences, Utrecht University, Utrecht, the Netherlands, ²TNO Applied Geoscience, Utrecht, the Netherlands, ³TNO Geomodelling, Utrecht, the Netherlands

Abstract This research targets disentangling shallow causes of anthropogenically induced subsidence in a reclaimed and urbanized coastal plain. The study area is the city of Almere, in the South Flevoland polder, the Netherlands, which is among the countries' fastest subsiding areas. The procedure consists of integrating Interferometric Synthetic Aperture Radar (InSAR) data with high-resolution phreatic groundwater and lithoclass models, and a database containing construction details. The InSAR data were derived from Sentinel-1, one ascending and one descending track, over a period from March 2015 until June 2020. The two main parts of the workflow are isolation of the InSAR points of structures without a pile foundation and a data assimilation procedure. The shrinkage of surficial clay beds by phreatic groundwater level lowering is identified as the main cause of subsidence in the area, with an average contribution of 6 mm per year. The history-matched physics-based model predicts that 1 m drop in phreatic groundwater level now translates into 10 mm of subsidence in the next 5 years. Additionally, a groundwater deficiency due to severe dry periods should be considered as an accelerator of subsidence. To ensure a robust network to estimate subsidence, we recommend a consistent monitoring strategy of the phreatic groundwater level.

Plain Language Summary The city of Almere, in the Netherlands, is part of a polder that was reclaimed in 1968. Land reclamation is accompanied by the lowering of groundwater levels, which can cause land subsidence. Almere is situated on top of about 9 m of soft soil layers. These layers were deposited after the last ice age and consist predominantly of clay and peat. It is important to understand and quantify the subsidence processes in these Holocene layers, to be able to mitigate subsidence. By lowering the groundwater level, the soft soil layers are dried. Clay shrinks when it dries out and organic material (within peat) oxidizes. Lowering the groundwater level also causes the load of the layers below to increase, which can result in the compaction of the layers (reduction in size by pressing together). This study targets the behavior of these processes. Results of our study indicate that the shrinkage of clay is the dominant driver of subsidence in Almere. One meter lowering in groundwater level now results in approximately 1 cm subsidence in 5 years. To improve our understanding of the non-trivial link between groundwater fluctuations and subsidence, higher spatial-temporal resolution groundwater monitoring is required.

1. Introduction

Over half a billion people live in coastal plains and deltas threatened by anthropogenically induced subsidence, and this number is expected to increase in the foreseeable future (Neumann et al., 2015; Schmidt, 2015). Many anthropogenic subsurface activities in coastal areas and delta plains result in subsidence, thereby amplifying relative sea-level rise and flood risks, inflicting damage to infrastructure, and overall, reducing the viability of these low-lying areas (Dinar et al., 2021; Guo & Jiao, 2007; Syvitski et al., 2009). Examples of subsurface activities are resources extraction, such as groundwater (Jones et al., 2016) and deep hydrocarbons (Chaussard et al., 2013), and surficial processes related to land use, primarily phreatic groundwater level management (Koster, Stafleu, & Stouthamer, 2018), and sediment deficit (Eslami et al., 2019).

Some heavily populated coastal plains and deltas require engineered extension of their surface area by land reclamation to accommodate population growth and increase the surface area of arable land, for example, China, Belgium, Japan, Dubai, the U.S., and Singapore (e.g., Declercq et al., 2021; D. Li et al., 2022; Martín-Antón et al., 2016; W. Wang et al., 2014). When land is gained along sea or lake shorelines by drainage of open water,

VERBERNE ET AL. 1 of 23



Journal of Geophysical Research: Earth Surface

10.1029/2022JF007031

Methodology: Manon Verberne, Kay Koster, Aris Lourens
Project Administration: Kay Koster, Peter A. Fokker
Resources: Manon Verberne, Aris Lourens, Jan Gunnink
Software: Manon Verberne, Aris Lourens, Thibault Candela
Supervision: Kay Koster, Peter A. Fokker
Validation: Manon Verberne

Visualization: Manon Verberne
Writing – original draft: Manon
Verberne

Writing – review & editing: Manon Verberne, Kay Koster, Aris Lourens, Jan Gunnink, Thibault Candela, Peter A Fokker this in essence means exposing waterlogged sediments to the atmosphere, thereby instigating various subsidence processes, primarily by shrinkage, compaction, and oxidation of fine grained and organic deposits.

The dense population of Hong Kong, for instance, prompted the government to reclaim land since the nineteenth century. There, rates of subsidence are around 20 mm per year, resulting in major damage to the built environment by differential settlements (Sun et al., 2018; M. Wang et al., 2016). In Bangladesh, reclamation primarily serves the purpose of gaining arable land, resulting in subsidence rates up to 10 mm per year in these reclaimed areas. This catalyzes a rise in social inequality as especially low-income farmers are not able to cover adaptation costs for the negative effects of these high subsidence rates (Barbour et al., 2022; Steckler et al., 2022).

The Netherlands is a prime example of a country that has extended its coastal plains by land reclamation. In total, the Netherlands has 443 reclaimed former lakes located in its coastal plains, with a cumulative surface area of 3,123.60 km² (Schultz, 1983). The centuries-long tradition of reclaiming land, referred to as "polder," can be divided into three main periods of lake drainage. The first stage comprised the sixteenth to seventeenth century, when many small lakes within the back-barrier peatlands were drained with windmills. Second, in the nineteenth century, larger lakes in the coastal plain were drained with steam pumping stations. Finally, in the twentieth century, Lake IJssel, the country's largest lake that was created by the damming of a tidal inlet, was partly reclaimed, resulting in the largest polders of all: the Lake IJssel polders (Figure 1a).

The focus of this study is on understanding and predicting shallow causes of subsidence in the reclaimed urbanized South Flevoland Polder (430 km²), which is part of the Lake IJssel polders (Figure 1). The polder was created in 1968 by constructing a ring-dike around the water body to be reclaimed. This enclosed water body was subsequently drained until the water level dropped below the former lake's floor. Subsidence immediately commenced when the waterlogged deposits experienced aeration for the first time and pore water progressively evaporated (Barciela Rial, 2019; De Glopper, 1969). Ultimately, the polder has experienced locally 1–2 m of subsidence since its reclamation (De Glopper, 1973, 1984; De Lange, 2015; De Lange et al., 2012; Fokker et al., 2019).

Paradoxically, severe water pumping has been ongoing to this day, as it is required to keep phreatic water levels low, thereby preventing the polder from flooding due to its low-lying position relative to the adjacent Lake IJssel's water level and increasing the load-bearing capacity of the former lake floor. The area thus continues to subside as waterlogged sediments are progressively exposed to the atmosphere. Besides flood risks, differential subsidence in the urbanized areas of the South Flevoland polder causes stress on structures, which results in damage to the built environment, leading to major costs. This especially accounts for the "Regenboogbuurt," which is a neighborhood that onlaps the thickest sequence of soft soil deposits in the area (Maas, 2021). Additionally, the severe drought events that have been striking Northwestern Europe during recent summers pose the threat of accelerated subsidence to the area by loosing pore water from fine grained and organic deposits. To the best of our knowledge, no study has been reported on the effects of severe drought in South Flevoland, although Hoogland et al. (2020) showed that subsidence may be slowed down by proactively saturating shallow peat beds within the area. Understanding, quantifying, and predicting subsidence, both spatially and temporally, in the South Flevoland polder is therefore of immense importance from both a socio-economic and a hazard-prevention point of view.

The lowering of phreatic water levels in the South Flevoland polder results in shrinkage of clay and oxidation of peat in the unsaturated zone (i.e., above the annually averaged lowest phreatic groundwater level). Clay shrinks as water that is adsorbed to charged platy clay particles evaporates and admixed organic matter oxidizes (Barciela-Rial et al., 2020). This leads to volumetric loss and is largely irreversible. Peat oxidation involves the breakdown of organic components by microbial activity. It is completely irreversible and results in the emission of carbon dioxide (Koster et al., 2020). Further, there are subsidence processes in the saturated zone: the consolidation of clay and peat layers due to an increase in effective stress by lowering of hydrostatic pressure when phreatic water levels are lowered (De Glopper & Ritzema, 1994). Consolidation and oxidation have been addressed regularly in other areas in the Netherlands that experience shallow subsidence (e.g., Kooi, 2000; Van Asselen et al., 2009, 2018). On the contrary, shrinkage of clay in the context of subsidence has been poorly covered (Fokker et al., 2019). However, in other countries, subsidence by clay shrinkage is considered as a major issue. In France and Great Britain for example, potential damage to the built environment inflicted by clay shrinkage as a result of drought and climate change has been studied in terms of cost per annum in the light of the insurance industry for decades (e.g., Burnol et al., 2021; Charpentier et al., 2021; Pritchard et al., 2015). In addition, in Sweden, locally increased subsidence rates in an urban area were linked to the presence of clay, with the aid of Interferometric Synthetic Aperture Radar (InSAR) (Fryksten & Nilfouroushan, 2019).

VERBERNE ET AL. 2 of 23

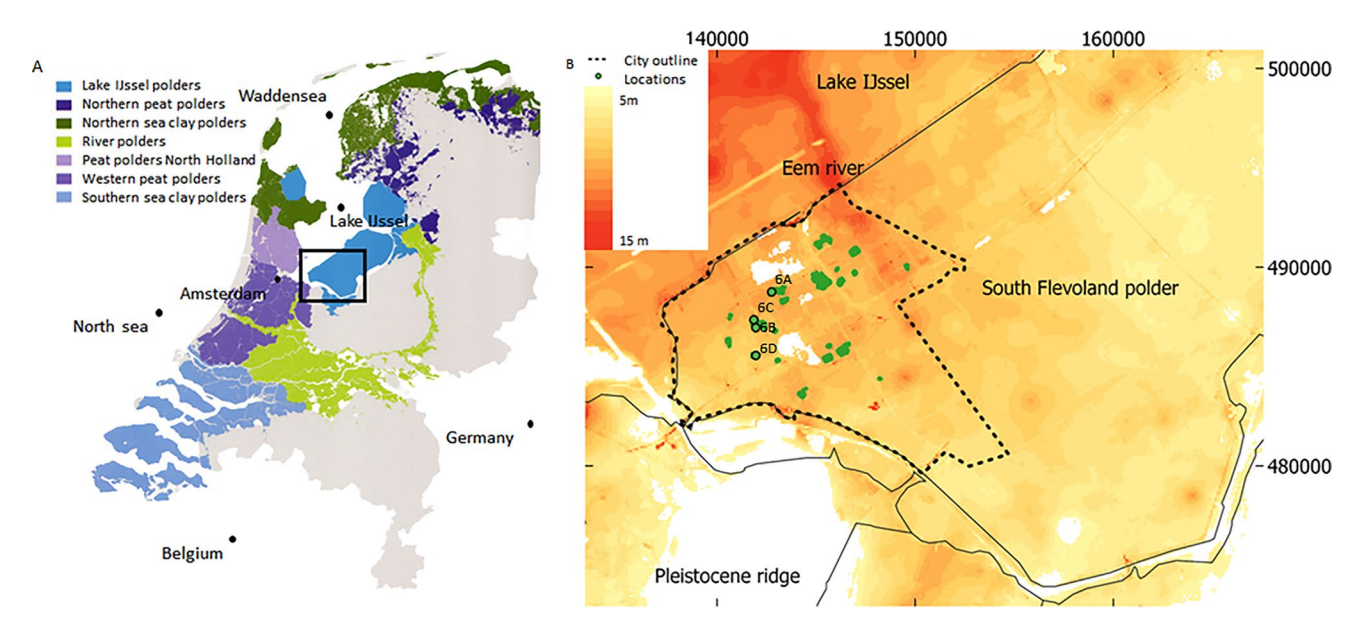


Figure 1. (a) Map of the Netherlands showing all the areas that accommodate polders (adjusted from Steenbergen et al. (2009)). (b) Map of the area of Almere and its surroundings projected on a map showing the thickness of the Holocene sequence (TNO, 2022). The thickness decreases toward the south-east. The incised course of the Eem River, in the northeast of the city Almere, is reflected by an increased Holocene thickness. The map is plotted on the Rijksdriehoek coordinate system. The green dots indicate the locations of the data points included in this study (see Figure 4). The locations of the graphs in Figures 6a–6d are denoted.

Most recent studies focus on establishing physics-based subsidence forecasts using input parameters derived by field- and laboratory measurements (Koster, Stafleu, & Stouthamer, 2018; Mayoral et al., 2017; Nusantara et al., 2018; Schothorst, 1982; Van Asselen et al., 2018). This approach inherently renders the subsidence estimates to be strongly dependent on used models and input soil parameters. A step forward regards the coupling of the different processes. Allison et al. (2016) for instance, stressed that developing an integrated model with coupled behavior of the different subsidence processes is critical for reliable subsidence estimates. Only by considering the behavior of all subsidence processes combined with real observations can the full impact of subsidence be understood.

Optimizing the relation between coupled subsidence processes and measured subsidence can improve subsidence forecasts. A history matching procedure by correlation and/or trial-and-error is often employed (e.g., Caló et al., 2017; Castellazzi et al., 2016; Teatini et al., 2006). For larger areas, or areas where multiple subsidence processes are superimposed, a more formal approach is considered more efficient (e.g., Candela & Koster, 2022; Fokker et al., 2019). A mathematically driven approach such as data assimilation can cover the entire range of uncertainty of all the parameters to seek the optimal solution.

Data assimilation combines models and observations to obtain the best possible description of the system (Evensen, 2009; Evensen et al., 2022). This approach is customary practice in a wide range of disciplines, such as subsurface modeling (Candela et al., 2022; Chang et al., 2010; Evensen et al., 2022; Fokker et al., 2016; Gazzola et al., 2021), weather predictions (Navon, 2009; Thépaut, 2003), and oceanographic simulations (Carton & Giese, 2008; Ghil & Malanotte-Rizzoli, 1991), but for interpreting shallow causes of subsidence this method has not yet been applied widely. Peduto et al. (2017, 2020) presented examples of shallow subsidence studies that apply a form of data assimilation to a geotechnical problem. Their studies show the benefit of combining multiple data sets. L. Li et al. (2017) applied data assimilation with an Ensemble Kalman Filter and showed the strength of data assimilation procedures, although they did not emphasize the subsidence models in their study.

Data assimilation procedures have also been applied in studies on polders in the Netherlands (Fokker et al., 2019; Muntendam-Bos et al., 2009). Fokker et al., 2019 used Ensemble Smoothing with Multiple Data Assimilation (ES-MDA) for 10 distinct locations in the South Flevoland polder with a few dozens of time steps over a period from reclamation until recent, combined with coring for lithological data and phreatic groundwater level measurements. They focused on the agricultural areas of the South Flevoland polder over a longer timescale with a small number of locations. Therefore, their results are not directly applicable to the subsidence in the urbanized

VERBERNE ET AL. 3 of 23

areas of the South Flevoland polder, where the urbanization might have had inhibitory effect on shrinkage and layers might have undergone more severe compaction in the past. Additionally, corings of individual locations were used in Fokker et al. (2019), whilst in this study we introduce an automated procedure including a lithological and groundwater model, making it possible to apply this methodology to larger areas.

Here, we aimed to quantify the subsidence processes within the Almere urban area of the South Flevoland polder in relation to phreatic groundwater level changes. Furthermore, we showcase the added value of combining large observational data sets with numerical models to improve parameter estimations for shallow subsidence processes. We deployed data assimilation on a data set comprising thousands of locations with hundreds of time steps derived from satellite observations, high-resolution 3D models of subsurface lithology and groundwater to quantify the contribution of the different shallow subsidence processes. We studied multiple subsidence processes at the same time to understand the full impact of subsidence and quantify the relative contributions of the different processes. Such information is critical for policymakers and spatial planners to design strategies to mitigate subsidence in the South Flevoland polder.

1.1. Study Area

The South Flevoland polder is situated in the central Netherlands in the partly reclaimed Lake IJssel (Figure 1). The Holocene sequence of the polder is underlain by several hundreds of meters thick Pleistocene sediments, consisting of a complex of alternating sandy to clayey marine, fluvial, and (peri-)glacial deposits (Menke et al., 1999; Peeters et al., 2015; TNO, 2022). The uppermost Pleistocene unit consists of a several meters thick aeolian sand bed, which grades from ca. -5 to -12 m below NAP (i.e., the Dutch ordinance datum, approximately corresponding to the mean sea level) in northwestern direction, locally incised by the Eem brook paleo-valley or elevated by dune formation (Figure 1).

During the Holocene, the South Flevoland Polder became part of the landward margin of a coastal plain. The base of the Holocene sequence consists of a basal peat bed formed between 6,000- and 7,000-year BP under the influence of inland groundwater level rise in tandem with post-glacial sea-level changes (Koster et al., 2017; Makaske et al., 2003). These peatlands drowned and transformed into an open tidal basin under the influence of continuous sea-level rise (Vos, 2015). The tidal basin deposits consist of alternating sand-clay beds, with local erosion of the underlying basal peat. When around 5,500-year BP eustatic sea-level rise decreased, the open tidal basin was closed off by the formation of a beach-barrier, transforming the area into a freshwater swamp with large-scale peat formation (Beets & Van der Spek, 2000; Makaske et al., 2003). In parallel, the area remained connected in the west to the North Sea by several smaller tidal inlets, making the Eem brook part of a branched network of freshwater tidal channels (Vos. 2015). The peatland itself was characterized by a series of open lakes (Menke et al., 1999). From the north, this lake system was connected to the Wadden Sea. When the peatlands deteriorated as a combination of natural and anthropogenic causes, the open sea connection in the north expanded southwards, thereby gradually drowning the peatlands and turning the area into a partly enclosed inland sea (Van den Biggelaar et al., 2014). The inland sea was dammed off and became Lake IJssel in 1932 to protect the surrounding areas against flooding. After the damming, several parts of the newly formed lake were reclaimed from 1939 onwards. The South Flevoland polder is the final area that was reclaimed.

Almere is a large urban conglomerate in the polder of South Flevoland (Figure 1), with a population of ca. 200,000. Almere was founded in 1976, approximately eight years after reclamation. This delay between reclamation and construction was used to account for the first years of subsidence, for which it was predicted to be the highest around Almere (up to 70 cm in total) (Hoeksema, 2007). Almere has been partly built on top of the paleo-valley of the Eem brook system, which incised several meters into underlying deposits of Pleistocene age. Therefore, the thickness of the Holocene sequence underneath Almere strongly varies, with thicknesses between <1 and 10 m. The thickest sequence can be found over the course of the former Eem brook system. Generally, basal peat in the Netherlands, like underneath Almere, has undergone substantial compression by the overburden, and consequently has mechanical characteristics that deviate from the younger peat beds (Koster, De Lange, et al., 2018). Due to sea-ingressions that drowned the peatlands, the paleo-valley infill on top of the basal peat consists of marine clay with sandy infills overlain by organic clay, gyttja and peat, interfingered with some sand (Menke et al., 1999).

VERBERNE ET AL. 4 of 23

Subsidence was expected after reclamation (De Glopper, 1969); therefore, regular monitoring campaigns were conducted, including regular leveling measurements, corings, and soil sampling (De Glopper, 1984; Van Dooremolen et al., 1996). Within 25 years, the a priori expected subsidence for the South Flevoland polder was exceeded, in some places, by 0.5 m (Van Dooremolen et al., 1996), resulting in complications for the drainage of the area. Most buildings have a concrete pile foundation in sandy, less compressible layers of Pleistocene age, and consequently do not subside in parallel with the overlying Holocene sequence. On the contrary, public structures, such as (local) roads, squares, sport fields, and playgrounds are often lacking a pile foundation and are constructed immediately on top of the Holocene sequence. The consequential differential subsidence between structures with and without a concrete pile foundation inflicts stress on pipeline structures, belowground electrical and network cables, and the connection from buildings to the roads in general, potentially causing damage. Currently, the city of Almere, lying ~4 m below NAP, must deal with damage to buildings and infrastructure because of the ongoing differential subsidence (Lambert et al., 2016).

2. Materials and Methods

We used a data assimilation procedure combining InSAR data with 3D lithological and phreatic groundwater level models. Figure 2 depicts the complete workflow, with the different colors indicating the different steps. In green, three classes of input data are displayed: (a) data in the form of previously developed geological and groundwater level models (Sections 2.1.3 and 2.1.4), (b) estimates of input parameters necessary for the forward model, based on a literature search (Section 2.2), and (c) satellite data for actual surface movement estimates (Section 2.1.1).

We defined three steps of the subsidence estimation algorithm:

- 1. The postprocessing of the InSAR data to filter the appropriate measurements points from the full data set (Section 2.1).
- 2. The forward model in which we calculated subsidence for all locations and time steps in this study (Section 2.2).
- 3. The data assimilation step, where the subsidence measurements derived from InSAR were combined with the forward model, to optimize the forward model by changing the input parameters (Section 2.3).

Finally, the output of our analysis is defined into two classes: (a) refined estimated parameters. As a result of the data assimilation approach, refined estimated parameters are the optimized values for the input parameters and (b) a subsidence prediction. The outcome of the forward model is a subsidence prediction for all the locations and time steps.

2.1. Input Data

2.1.1. InSAR Data

The InSAR data consists of Sentinel-1 images for one ascending and one descending track, ranging over the period March 2015 until June 2020 and November 2015 until June 2020, respectively. The sampling interval of the data points varies temporally by the availability of the 6-day repeat pass for the period until April 2016 and the 12-day repeat pass from April 2016 onwards (Wegmüller et al., 2015). The data used for our analysis are processed InSAR data retrieved from Rijkswaterstaat (2022). It consists of point-wise time series of both persistent and distributed scatters. For details on the processing steps of the provided data, see Rijkswaterstaat (2018). We recognize that this data has been processed for nationwide purposes, which can potentially be an additional source of error when applying the data set on a local or regional scale. This has been taken into account with a relatively large noise to our InSAR data in the data assimilation process, compared to the accuracy levels described in Rijkswaterstaat (2018).

The ascending and descending tracks were processed and analyzed separately. This yielded two results of subsidence estimations and associated fits, which were compared for an additional quality check of the workflow. The line-of-sight movement was projected to the vertical direction with the use of the incident angle as part of the processing; $m_v = \frac{m_{LOS}}{\cos x}$. This was done with the assumption that the horizontal movement is negligible. The map of the European Ground Motion Service (Costantini et al., 2021) gives some indication of horizontal movement in the area, but all the points with East-West movement appear to be in the vicinity of founded structures. Manually checked points on top of sportfields do not show significant East-West movement. After our InSAR point

VERBERNE ET AL. 5 of 23

21699011, 2023, 7, Downloaded from https://agupubs.onlinelibrary.wiley.com/doi/10.1029/2022/H007031 by Cochrane Netherlands, Wiley Online Library on [03/07/2023]. See the Terms

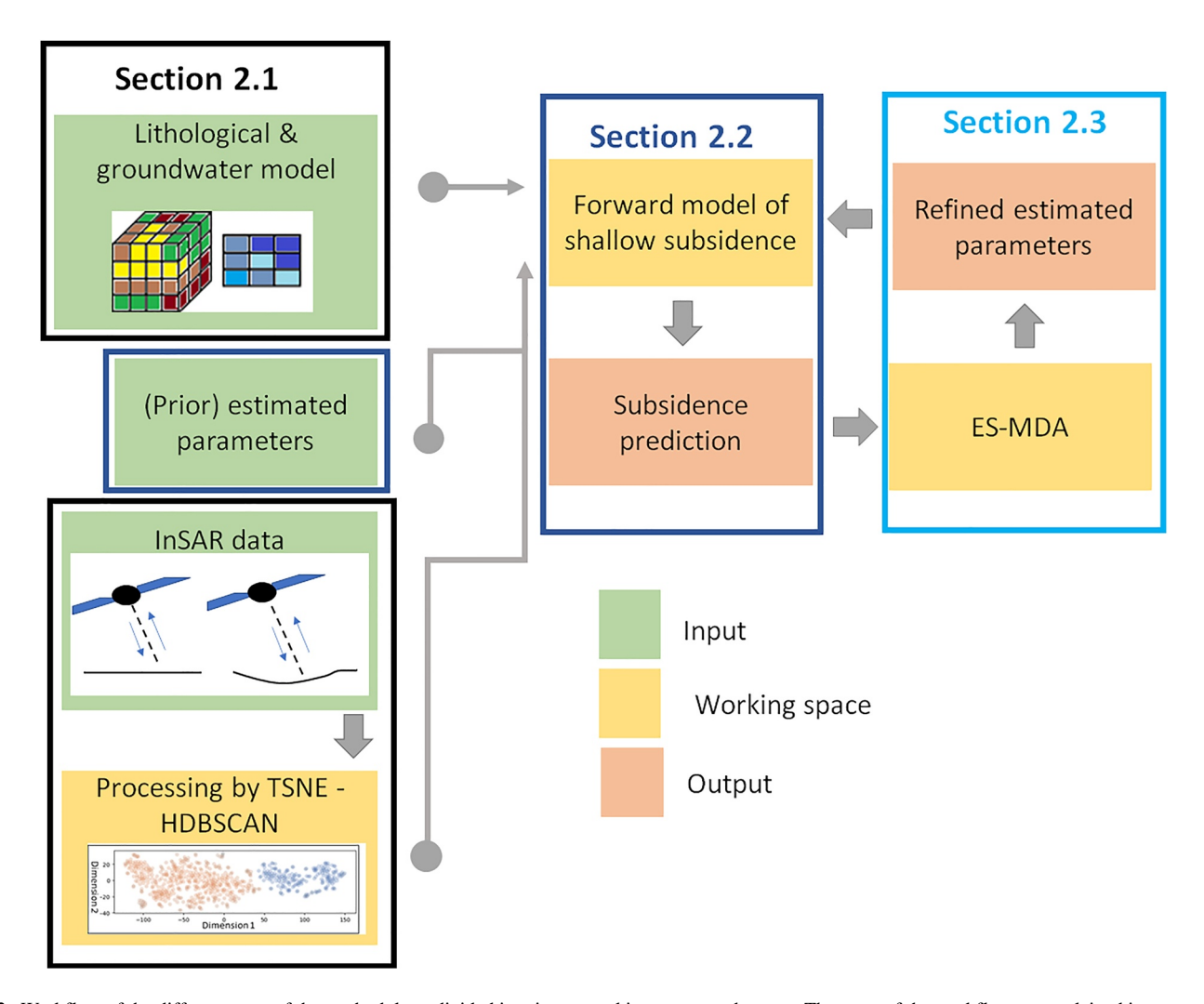


Figure 2. Workflow of the different steps of the methodology divided into input, working space, and output. The steps of the workflow are explained in corresponding sections. The parameters of the physical models that estimate subsidence are optimized toward measured relative subsidence from satellite data, with the use of a groundwater model and a lithological model. Interferometric Synthetic Aperture Radar points measured on top of unfounded objects are separated by a data selection process (Figure 3). A prior estimate of the parameters part of the forward model is initially made, whereafter the forward model and optimization with data assimilation are repeated multiple times. The image of the lithological grid model is adjusted from Van der Meulen et al. (2007).

selection, both the ascending and descending tracks show similar rates of subsidence in the vertical direction, indicating that there is no significant horizontal movement. Additionally, we do not expect them because of the shallow character of the cause of subsidence.

One of the key issues of InSAR data is the loss of signal coherence, both in space and time. Spatial decorrelation is caused by changes in the acquisition baseline, resulting in a different phase between two images and causing phase unwrapping errors that reduce the coherence. This implies that spatially decorrelated data are less suitable for subsidence research. Temporal decorrelation is caused by atmospheric variability and changes in the physical and geometric properties of the scatter points, for example, due to seasonal changes in vegetation which result in land cover changes (Ferretti et al., 2007; Hanssen, 2001). As a result, vegetation-rich areas are suboptimal for the analysis of subsidence by satellite imaging (Conroy et al., 2022). Therefore, the point-wise time series of the provided InSAR data are largely located on man-made structures because these scatter points face less decorrelation issues. In this study, we aim to understand the subsidence behavior of the Holocene layers, and as a large part of the man-made structures have pile foundation, we applied an additional postprocessing workflow to the InSAR data to select points that are not on top of pile founded structures. This workflow is explained in Section 2.1.2.

VERBERNE ET AL. 6 of 23

21699011, 2023, 7, Downloaded from https://agupubs.onlinelibrary.wiley.com/doi/10.1029/2022/H007031 by Cochrane Netherlands, Wiley Online Library on [03/07/2023]. See the Terms and Conditions (https://onlinelibrary.wiley.com/terms-and-conditions) on Wiley Online Library for rule

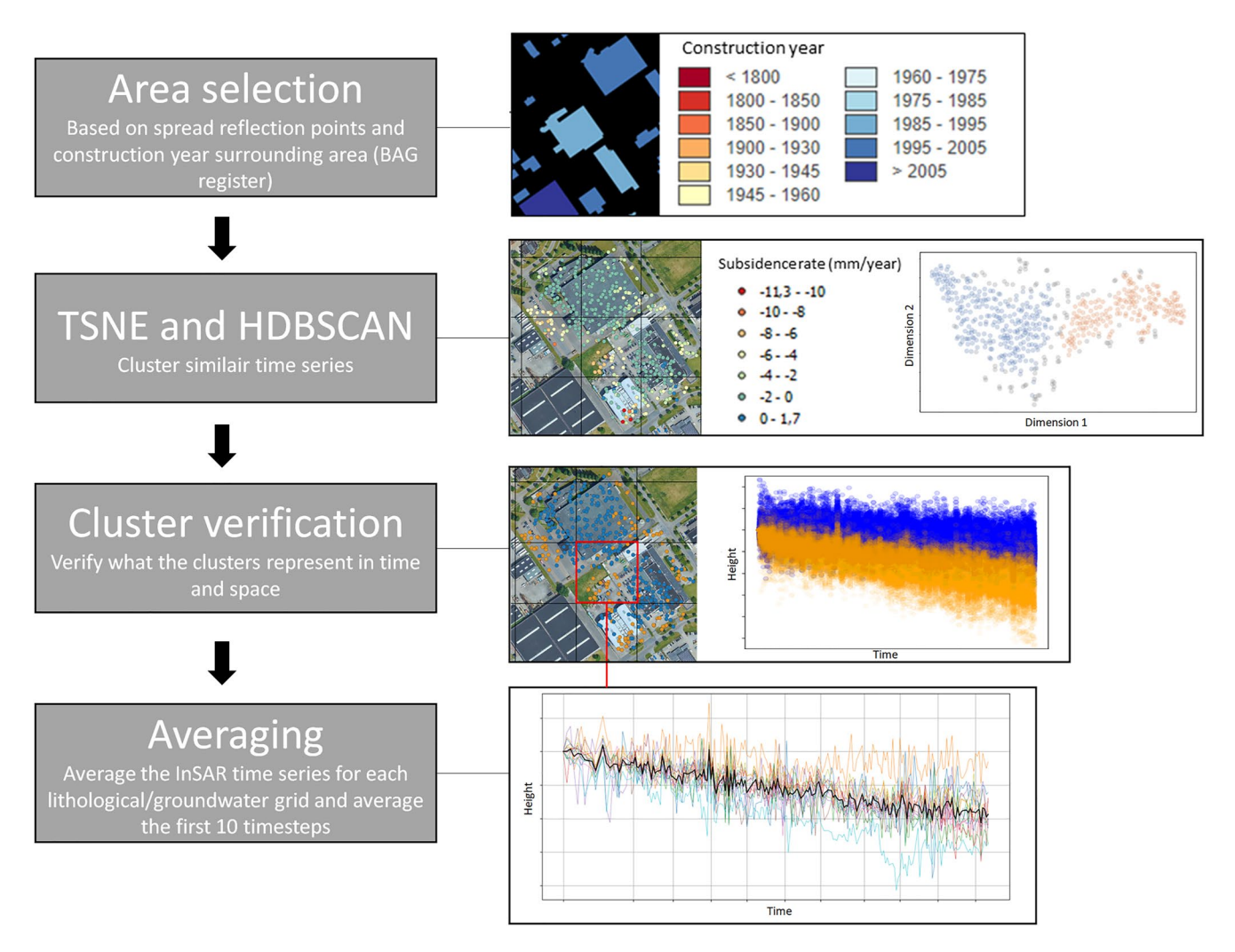


Figure 3. Workflow for selecting Interferometric Synthetic Aperture Radar (InSAR) points. First, areas with a significant amount of data points, potentially on top of the structure without a pile foundation, are selected. With the Basisregistratic Adressen en Gebouwen register (Kadaster, 2022), the construction date of the area is verified. The image shows the construction years of the buildings in the example area (image adjusted from Spaan (2015)). The remaining areas follow dimensionality reduction by time Distributed Stochastic Neighbor Embedding (T-SNE), followed by a clustering method Hierarchical Density-Based Spatial Clustering of Applications with Noise. At the second processing step, the average yearly subsidence rate of the selected InSAR points of the sample area is shown on the left. On the right, the result of the T-SNE dimension reduction is plotted, where the colors refer to the clusters each point is assigned to. The number of dimensions of the initial data set is equal to the number of locations. Third, the clusters are visualized as scatter points for each time step and in a geographic information system to verify the clusters and select the cluster representing the scatter points on top of unfounded man-made structures. The clusters from the second time step, in their corresponding colors, are plotted spatially on the left image and over time on the right. Finally, for each grid cell corresponding to the lithological and groundwater model, an average of the selected InSAR points within the cell is taken. This is depicted in the graph belonging to the last processing step, where the thick black line represents the average of the InSAR time series falling into the grid cell. To not give a disproportionate high weight to the first measurement of the InSAR series, an average has been taken of the first time steps, which forms the first time step in our post processing time series.

2.1.2. InSAR Processing by TSNE-HDBSCAN

InSAR locations were selected based on two main criteria, forming the first step in the point-selection procedure of Figure 3. We selected PS-InSAR points in the built-up area of Almere without a pile foundation. Buildings in the area typically have a pile foundation reaching depths of ca. 7–20 m with respect to NAP, that is, piles driven in Pleistocene sand beds with load bearing capacity (Spikker, 2010). Consequently, buildings with a pile foundation are less suitable to reflect subsidence processes that happen within the Holocene sequence. We therefore focused on large reflective objects (more than 10 reflection points) without pile foundations. These objects range from large parking lots around shopping centers and business parks to playgrounds, concrete sport fields, and artificial grass turfs.

VERBERNE ET AL. 7 of 23

The next selection criterium was that the structures without foundations had been built at least 10 years before the first InSAR acquisition dates. Therefore, only objects constructed before the year 2005 were considered. This choice was made to reduce the effect of consolidation due to construction of the objects without foundations on the subsidence signal. Because no register exists for the construction date of parking lots, playgrounds, and sport fields, the year of construction of the associated buildings was used. The construction year of all buildings in the Netherlands are registered in "Basisregistratic Adressen en Gebouwen" (BAG) (Kadaster, 2022), which was used to verify the construction year of objects in the selected areas.

Reflection points on top of structures without a pile foundation that meet above stated criteria were isolated from the ones on top of structures with a pile foundation using a statistical visualization method. First, data points were separated with time Distributed Stochastic Neighbor Embedding (Van der Maaten & Hinton, 2008), subsequently data points were appointed to a cluster using Hierarchical Density-Based Spatial Clustering of Applications with Noise (HDBSCAN) (Campello et al., 2013). This two-steps approach based on unsupervised machine learning enables isolating time series that measure the same processes. In the case of Almere, no significant subsidence below the level of the pile foundations was expected. Hence, objects with a pile foundation should show negligible subsidence, whereas other nearby objects without a foundation were expected to show subsidence. This would result in differently behaving timeseries for points measured on top of objects with and without a pile foundation. This step formed the second step in the point selection procedure of Figure 3.

The practice of dimensionality reduction followed by clustering is common for large input data and has been applied to SAR data sets (Van de Kerkhof et al., 2020), and for a wide range of other data types (Fernández Llamas et al., 2019; R. Harrison et al., 2019; Kahloot & Ekler, 2019). T-SNE is a dimensionality reduction method that can group similarly behaving time series of height measurements of the different reflection points (Van der Maaten & Hinton, 2008). For the present study, clustering was conducted with HDBSCAN. HDBSCAN provides significant clusters, where the clusters can vary in density threshold. The method maximizes the stability of the selected clusters by calculating the optimal solution (Campello et al., 2013).

To ensure that the selected clusters represent the time series of measurements on top of objects without a pile foundation, the clusters were verified by checking the time series of all the clusters and their location in a geographic information system. This is the third procedure of Figure 3. Figure 4 shows all the resulting InSAR points selected for both the ascending and descending tracks in map view. The processed InSAR data can be found in Data Sets S2 and S3 of this paper.

The last step in Figure 3 entails the optimization of the selected InSAR points for the subsidence optimization procedure. InSAR data points in a single lithological grid cell (see Section 2.2. about lithological modeling) were averaged. Reducing the number of points by averaging reduces the computational time, while still incorporating the uncertainty for the InSAR data for each grid cell. The variance of this average was added to the chosen standard deviation squared of 0.01 m² to ensure that the uncertainty of variance in the subsidence measurements was incorporated. A 0.01 m² standard deviation for each epoch aims to capture both the uncertainty in the model and measuring space, as the true standard deviation is unknown. To prevent a disproportionate weight of the first measurement in time, an average of the first 10 measurements in time was taken as the first time step in our post-processing time series data.

2.1.3. Lithoclass Model

Previously released 3D lithoclasses (classes of different grainsize compositions) voxel model for the province of Flevoland that covers the entire study area was used as input for numerical modeling (Figure 5a) (Gunnink, 2021). The model was initially developed for high-resolution hydraulic resistance modeling for groundwater flows within the Holocene sequence, and was constructed based on 31.000 digitalized borehole logs and 4,250 Cone Penetration Tests derived from the freely accessible online data portal of the Geological Survey of the Netherlands (TNO-GSN, 2022). The boreholes are sufficiently distributed throughout the province of Flevoland, whereas the Cone Penetration Test is primarily clustered in urbanized areas and along infrastructural elements.

The 3D model was created by interpolation via spatial kriging, following a similar procedure as explained in Van der Meulen et al. (2013). The voxel x, y, z dimensions are $100 \times 100 \times 0.5$ m and the model ranges from the surface to the top of geological units of Pleistocene age, thereby encompassing the entire Holocene sequence. The different lithoclasses (sand, sandy clay, clay, peat, and basal peat—the latter being in a more compressed

VERBERNE ET AL. 8 of 23



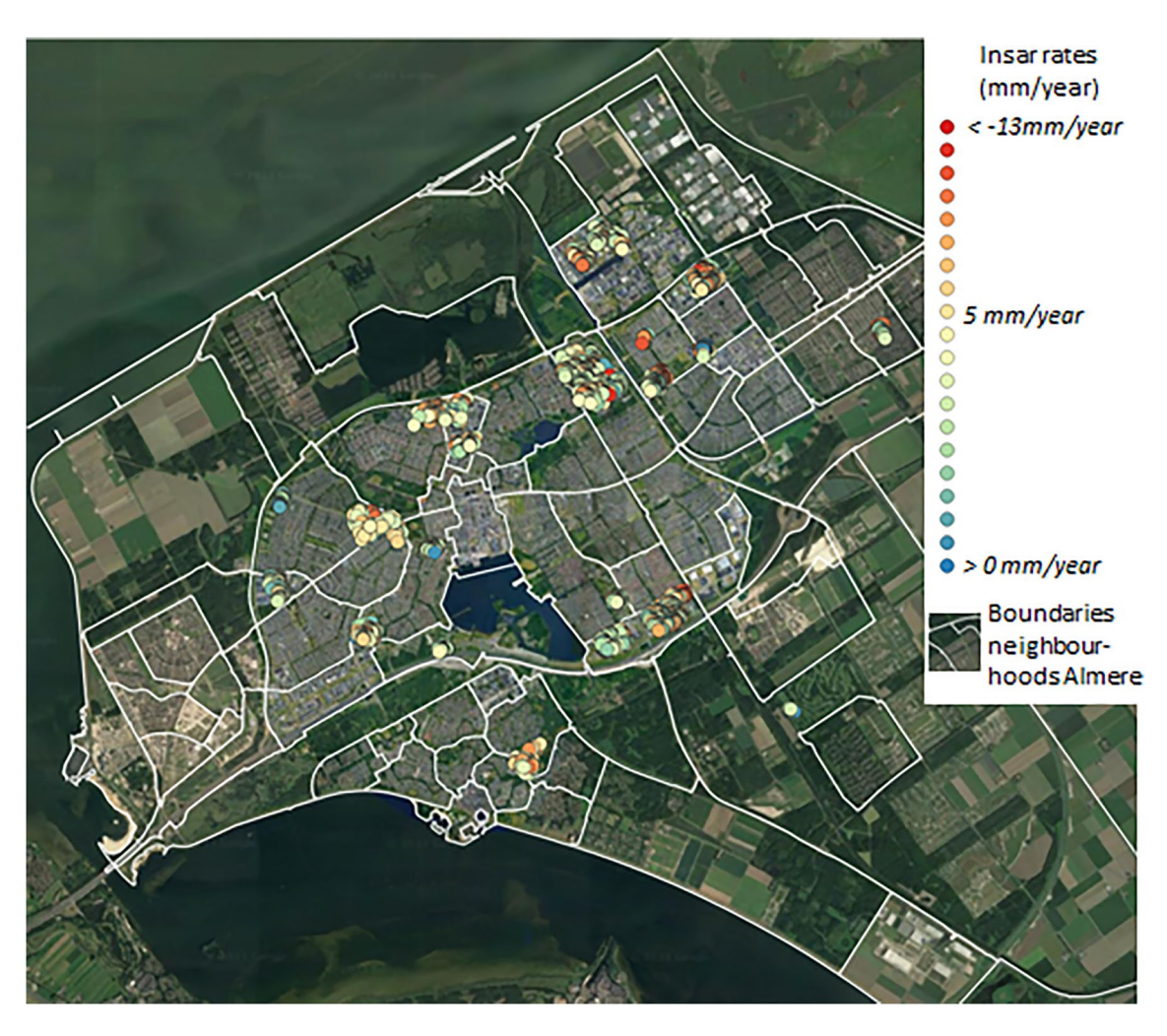


Figure 4. Map view of the selected Interferometric Synthetic Aperture Radar points after the time Distributed Stochastic Neighbor Embedding and Hierarchical Density-Based Spatial Clustering of Applications with Noise selection procedure for both the ascending and descending tracks on top of a satellite image (Google, 2023). To aid in the visualization of the area, the boundaries of all the neighborhoods in Almere (CBS, 2020) are plotted.

state than peat) are described with their probability of occurrence for each voxel, based on 100 realizations of the interpolation. The highest probability was taken as the truth scenario for this study.

2.1.4. Groundwater Model

Changes in groundwater heads form an important explanatory variable for shallow sources of subsidence. Therefore, time series of these data are needed all over the study area. Unfortunately, this was only sparsely available at locations with observation wells. Therefore, a model was developed to estimate the required time series (TNO-GSN, 2022; Zaadnoordijk et al., 2018): monthly phreatic water level values for grid cells of x, y 100×100 m (Figure 5b) from the year 2000 to 2020. The applied method was an interpolation in two steps. The first step was an interpolation of the groundwater heads within the time series to obtain for all well locations an observation on the same day (28th) of each month. This yielded interpolated heads including variances. The second step comprised a spatial (kriging) interpolation, applying a sequential Gaussian simulation (Deutsch & Journel, 1998), which yielded for each month a map of the interpolated heads. Since the observation wells were sparse, their observed heads could not fully describe the spatial variation in the groundwater heads. Therefore, a trend surface was used with a spatial interpolation performed on the residuals (observation minus trend surface). To honor the seasonal fluctuation of the groundwater heads, each month had a separate trend surface. Herewith, one hundred equiprobable interpolations of phreatic groundwater levels for each month were created. We used the average of the 100 realizations as the truth scenario for the phreatic surface model in space and time. The exact well locations can be found in Data Set S1 of this paper.

VERBERNE ET AL. 9 of 23

21699011, 2023, 7, Downloaded from https://agupubs.onlinelibrary.wiley.com/doi/10.1029/2022/H007031 by Cochrane Netherlands, Wiley Online Library on [03/07/2023]. See the

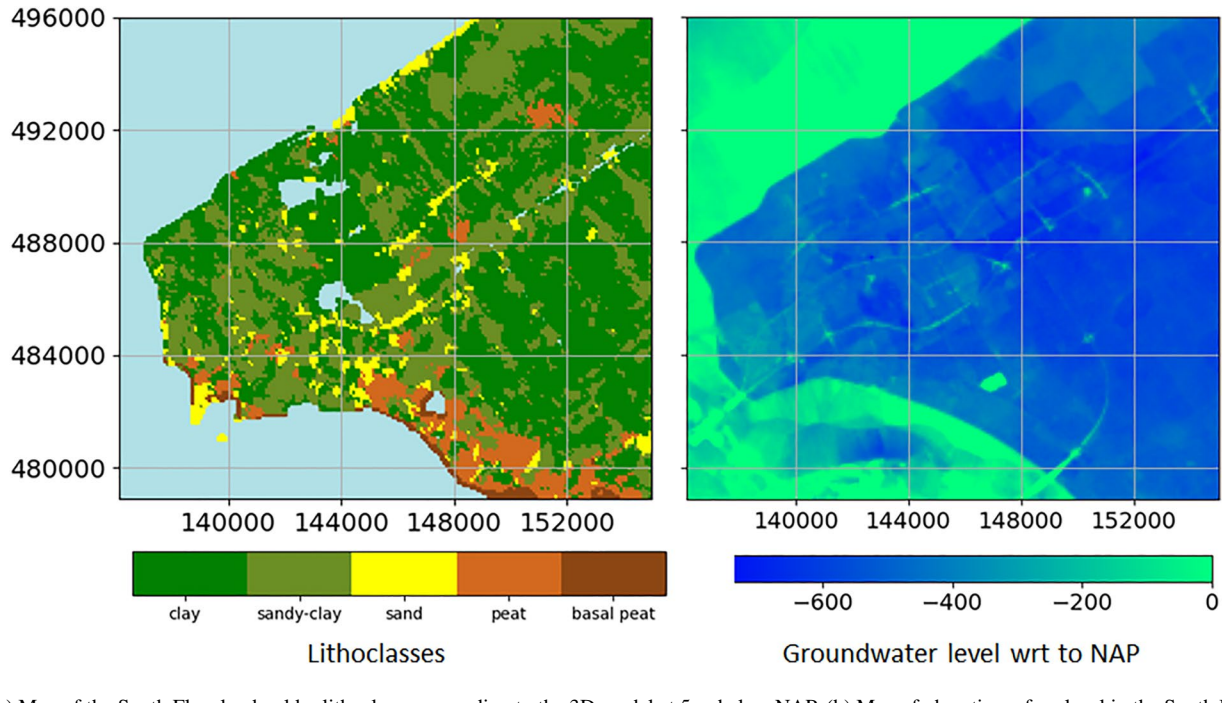


Figure 5. (a) Map of the South Flevoland polder lithoclasses according to the 3D model at 5 m below NAP. (b) Map of phreatic surface level in the South Flevoland polder in January 2015. The scale is in cm with respect to NAP. The polder itself lies ~400 cm below NAP. The areas that lie at NAP are the Lake IJssel area and in the bottom left of the mainland.

2.2. Forward Model

The different shallow subsidence processes initiated by human-induced phreatic groundwater level lowering in the South Flevoland polder are described in forward models. These forward models include physical relations that describe the subsidence processes and thereby, with an estimate of the parameters, provide an estimate of the subsidence. The groundwater and lithoclasses models are used to describe which lithology is present and to what depth the sediments are saturated. Previous studies identified oxidation of peat, shrinkage of clay, and compression of clay and peat as the main subsidence processes in the area (De Lange et al., 2012; Fokker et al., 2019; Lambert et al., 2016; Van Dooremolen et al., 1996).

Fokker et al. (2019) described a subsidence model with a relation between shrinkage and equivalent age using linear-strain fits and time series of land leveling subsidence observations in the South Flevoland polder from 1967 to 2012. They used an exponential relation of clay shrinkage processes to fit the model to the data. Furthermore, they described that well-established compression functions of consolidation and creep (Den Haan, 1996; Viscchedijk & Trompille, 2009) did not fit with the observed subsidence trend. Given the results of the study of Fokker et al. (2019), subsidence by compression was expected to be negligible in comparison to the processes of shrinkage and oxidation for the timing after reclamation and due to the length of our study period. Therefore, we have not modeled compression as a separate process in this study. Note also here that compression by the overburden weight of building material was assumed to have a negligible effect on the selected InSAR time series because all the locations included in this study have undergone settlement due to loading by construction for minimal 10 years (cf. CUR, 1992).

2.2.1. Oxidation Model

The applied equation for the oxidation model is widely used to describe peat oxidation in the Netherlands (Fokker et al., 2019; Koster, Stafleu, & Stouthamer, 2018; Van den Akker et al., 2008; Van der Meulen et al., 2007; Van Hardeveld et al., 2017). It provides a relative annual oxidation rate for peat above the phreatic groundwater level. Since only organic matter oxidizes, admixed sediments remain, albeit on average only 3%–4% of the total volume (Koster, Stafleu, et al., 2018). Hence, a residual thickness is considered.

First, for a unit above the phreatic groundwater level, the part susceptible to oxidation needs to be determined.

VERBERNE ET AL. 10 of 23

If part of a unit has already been reduced, we have $h_{ox}(t) = h(t) - R_{r,ox}h_0$. The original thickness of the unit is unknown, since the collection of the data used in this study started ~50 years after reclamation. Hence, we simply assumed h equals h_0 at t = 0. This results in a higher residual height than for completely virgin soil, as the original units are (partly) reduced in thickness already. The oxidation rate can be calculated as follows:

$$\frac{dh}{dt} = \frac{dh_{ox}}{dt} = -V_{ox} h_{ox} \tag{2}$$

Over time Δt the thickness reduction of a layer can be written as follows:

$$\Delta h = h_{ox}(t) - h_{ox}(t + \Delta t) = \left(1 - e^{-V_{ox}\Delta t}\right) \cdot h_{ox}(t)$$

$$= \left(1 - e^{-V_{ox}\Delta t}\right) \cdot (h(t) - R_{ox}h_0)$$
(3)

Incorporating units that are partly aerated, the part susceptible of oxidation is corrected for the wet part of the voxel:

$$\Delta h_{ox} = \left(1 - e^{-V_{ox}\Delta t}\right) (h(t) - h_{wet} - R_{ox} \left[h_0 - h_{wet}\right]) \tag{4}$$

In which V_{ox} is the shrinkage rate and R_{ox} is the residual height.

2.2.2. Shrinkage Model

Time-dependent shrinkage models have not been documented for the Netherlands yet. Typically, shrinkage is expressed as a function of clay mineral content, organic matter, and calcareous admixture (e.g., Barciela Rial, 2019; De Glopper, 1969). To overcome this, Fokker et al. (2019) designed a simple shrinkage relation, inspired by Equation 4, which enabled good matches between the subsidence model and the observed subsidence. This relation assumes that the shrinkage rate is proportional to the volume sensitive to shrinkage. A lithology-dependent residual height was assumed to indicate an asymptotic value to which the shrinkage can lead.

The process of clay swelling has been ignored in this study. Furthermore, seasonal swelling effects of clay by a relative increase in precipitation during autumn and winter were not observed in the InSAR data. Most likely, if present, a swelling capacity is suppressed in the urbanized area by structure overburden. In general, the South Flevoland polder is subjected to net phreatic groundwater level lowering; this is reflected in net subsidence, visible as a decreasing trend without a large swelling effect in the InSAR data. Furthermore, previous studies reported that the clay beds in our study area have a relatively high irreversible character regarding shrinkage (Bronswijk & Evers-Vermeer, 1990; Kim et al., 1993).

The equation for shrinkage (Equation 5):

$$\Delta h_{sh} = (1 - e^{-V_{sh}\Delta t})(h(t) - h_{wet} - R_{sh}[h_0 - h_{wet}])$$
(5)

In which V_{sh} is the shrinkage rate and R_{sh} is the residual height.

2.2.3. The Prior Estimated Parameters

The parameters aimed to optimize are the shrinkage and oxidation rate and their respective residual heights (see first column of Table 2). The prior estimated values take into account the results of Fokker et al. (2019). The rates were lowered because a significant amount of time (~50 years) has passed since reclamation (and the start of the study of Fokker et al. (2019)), decreasing the void ratio of deposits and increasing the stiffness. Additionally, there is a potential inhibitory effect of shrinkage and oxidation rate in the urbanized area, compared to the agricultural area of Fokker et al. (2019).

The rates of shrinkage and oxidation are closely related to the associated residual heights. Due to the brief period of the surface elevation data (~5 years), the exponential relation between relative residual height and reduction (shrinkage or oxidation) rate cannot be established absolutely: an increase in subsidence rates can have the same effect on total subsidence as a reduction in residual height. As a result, the contribution of relative residual height

VERBERNE ET AL. 11 of 23

and reduction cannot be distinguished. If one of the two parameters increases, the other should increase as well, to reach the same value for total subsidence. From Equations 1 and 2, we can derive the following equation:

$$\frac{dh}{dt} = h_0 v \left(1 - R\right) e^{-vt} \tag{6}$$

Therefore, if a certain height reduction rate is acting, it can be the result of different combinations of v and R, as long as the right-hand side of Equation 10 gives the same number. The exponential in this equation can be neglected because the compaction (order of mm) is very small with respect to the layer thickness (order of m). Different combinations with the same value of C = v(1 - R), or $R = 1 - \frac{C}{v}$ therefore, give equally good fits, with no time dependence in the expression. This equation was hence fitted to the posterior result of the residual height and rate of oxidation and shrinkage for the different lithologies, utilizing automated least squares polynomial fit.

2.3. ES-MDA

Parameters have been estimated with Ensemble Smoother with Multiple Data Assimilation (ES-MDA) (Emerick & Reynolds, 2013; Evensen et al., 2022). Earlier accounts for the method to estimate parameters for shallow subsidence can be found in Fokker et al. (2019); the method has also been applied to estimate the parameters for deep subsidence processes (gas production) (e.g., Fokker et al., 2016; Gazzola et al., 2021).

An ensemble refers to a collection of members that are the result of a Monte Carlo analysis. Members are single realizations of the model with specific values for the different parameters. ES-MDA is thus based on a parameter description of the properties that describe the physical processes in the subsurface. A forward model takes the parameters and calculates the subsidence in space and time for each member of the ensemble. The ES-MDA algorithm minimizes the mismatch between the measured data and the estimated subsidence values by changing the parameters of the ensemble members in an organized manner. The multiple data assimilation notion of ES-MDA indicates that the assimilation process is repeated several times. The newly estimated parameters are taken to create a new ensemble of members, with each step increasing the confidence in the parameters.

ES-MDA can be mathematically described as follows. The parameters collected form the vector \mathbf{m} . The subsidence data are put into a vector \mathbf{d} , this vector has the length of the number of data points in the area multiplied by the time steps taken at each location. Operation of the forward model is indicated by $\mathbf{G}(\mathbf{m})$; it calculates the subsidence as a function of time for each individual location, based on the parameters in \mathbf{m} . We want to estimate the vector \mathbf{m} for which $\mathbf{G}(\mathbf{m})$ has the smallest misfit with the data \mathbf{d} . To do so, for a single member, a set of prior parameters is created (\mathbf{m}_0), with covariance in a matrix $\mathbf{C}_{\mathbf{m}}$. Another covariance matrix is created for the data ($\mathbf{C}_{\mathbf{d}}$). Following Tarantola (2005), the least squares solution is acquired by maximizing J in the following function:

$$J = \exp\left(-\frac{1}{2}[m - m_0]^T C_m^{-1}[m - m_0] - \frac{1}{2}[d - G(m)]^T C_d^{-1}[d - G(m)]\right)$$
(7)

In the ensemble procedure, the values of the members are derived from a prior estimate with a standard deviation of the parameters. An ensemble consists of N_e vectors of \mathbf{m} ; $\mathbf{M} = (\mathbf{m}_1, \mathbf{m}_2, ..., \mathbf{m}_{N_e})$. Similarly, an ensemble of data vectors is created by adding random noise to the data following the uncertainty of the data points: $\mathbf{D} = (\mathbf{d}_1, \mathbf{d}_2, ..., \mathbf{d}_{N_e})$.

To solve the least squares solution for the entire ensemble at once, GM replaces G(m) in Equation 5. GM is the result of the parameters of all ensemble members operating in the forward model and is the collection of realizations of surface elevations through time. GM' is defined as the difference between GM and the average of GM. M' is the difference with the prior mean for each ensemble member: $M' = M - m_0$. The covariance matrix is defined as $C_m = M' M'^T / (N_e - 1)$. The new set of parameters for the ensemble is given by the following equation:

$$\hat{\boldsymbol{M}} = \boldsymbol{M} + \boldsymbol{M}' \left[\mathbf{G} \mathbf{M}' \right]^T \left(\mathbf{G} \mathbf{M}' \left[\mathbf{G} \mathbf{M}' \right]^T + (N_e - 1) \boldsymbol{C}_d \right)^{-1} (\boldsymbol{D} - \boldsymbol{G} \boldsymbol{M})$$

$$= \boldsymbol{M} + \boldsymbol{M}' \left(\left[\boldsymbol{G} \boldsymbol{M}' \right]^T \boldsymbol{C}_d^{-1} \boldsymbol{G} \boldsymbol{M}' + (N_e - 1) \mathbf{I} \right)^{-1} \left[\boldsymbol{G} \boldsymbol{M}' \right]^T \boldsymbol{C}_d^{-1} (\boldsymbol{D} - \boldsymbol{G} \boldsymbol{M})$$
(8)

Depending on the number of parameters versus number of data points, one of the two equivalent expressions might be more appropriate to use. $\hat{\mathbf{M}}$ is the estimated ensemble of parameters.

VERBERNE ET AL. 12 of 23

Table 1 Parameters for the Data Assimilation Procedure of This Study			
Number of ensemble members (–)	200		
Number of assimilations (-)	4		
q (-)	0.667		
Covariance data (m)	0.01		
Number of InSAR data points (-)	3,747 (descending), 2,846 (ascending)		
Number of voxel locations (-)	199 (descending), 158 (ascending)		
Number of points in time (–)	208 (descending), 212 (ascending)		
Number of model parameters	6		

The ensemble smoother technique with a new estimate of parameters can be applied repetitively to obtain a better estimate of parameters in the case of non-linear forward models (Emerick & Reynolds, 2013). The set of parameters is updated with each subsequent step. The data remain the same over the entire procedure. To compensate for the effect of multiple applications with the same data, the covariance of the data is increased with each step of the optimization. This is done with a factor α_i , where the following condition is met: $\sum_{i=1}^{nI} \frac{1}{\alpha_i} = 1$. nI is the number of assimilation steps (Fokker et al., 2019). We used a factor α_i that decreases every step with a factor q to ensure increasing influence of subsequent assimilations.

$$\alpha_i = \alpha_0 \cdot q^i \tag{9}$$

With i being the assimilation step. The above summation condition is met with

$$\alpha_0 = \frac{1 - q^{nI}}{q^{nI - 1} - q^{nI}} \tag{10}$$

To verify the results and determine the actual improvement of the parameter estimation procedure, a test function is applied, considering the covariance of the data and the estimate parameters after the last assimilation step:

$$\chi^{2} = \left(\hat{\mathbf{G}}\mathbf{M} - \mathbf{d}\right)^{T} \left(\mathbf{C}_{d} + \mathbf{C}_{\hat{\mathbf{G}}\mathbf{M}}\right)^{-1} \left(\hat{\mathbf{G}}\mathbf{M} - \mathbf{d}\right)$$
(11)

The outcome of this equation should be around the degree of freedom (Nd), so that $\frac{\chi^2}{Nd} \approx 1$.

The parameters for this study are summarized in Table 1. The number of grid cells equals the number of lithological and groundwater voxel cells covered by the InSAR data points. In the result section, we present key examples of individual voxel cell locations, the values of the optimized parameters and correlations between different parameters.

3. Results

Our ES-MDA-based workflow yielded 357 individual scatter point locations. To provide a representative summary of the results on point location scale, we present four key examples below (Figure 6). These locations were chosen to represent the variance in lithoclass composition, which is dominated by clay and sandy clay, with occasionally sand and peat layers. Additionally, we present four key indicators for parameter covariance (Figure 8), values for the estimated parameters (Table 1), and the average contribution to subsidence for clay and peat (Table 2). The estimated parameters consist of the four model parameters for the shrinkage of clay (shrinkage rate and relative residual thickness for clay and sandy clay), and two model parameters for oxidation (oxidation velocity and relative residual thickness of peat).

The four key examples of the results of the simultaneous assimilation are presented in Figure 6. The time series of the prior ensemble is not indicated in Figure 6. Because they have a high variance, they would not fit into the scale of the figure. The red time series in Figure 6 are the 200 modeled surface movement developments for the ensemble of assimilated parameters. The black dots are the InSAR data points, and the gray area represents the uncertainty given to each data point, as described in Section 2.1. On the right y-axis in the same plot, the phreatic groundwater level variation is plotted. The lithological column and the location of the column with respect to the phreatic groundwater level are indicated on the right of the plot. The time series and the estimated subsidence correspond well, regardless of lithology, except for Figure 6a. The prior and estimated parameters are presented in Table 2.

Table 2 provides the estimates prior and posterior to the data assimilation with their standard deviation. Results are given for the descending and ascending satellite tracks separately. The two tracks provide comparable estimated parameters as a result of the data assimilation. The similarity of the results for the two tracks strengthens our assumption of no horizontal displacement. The outcome of the estimated parameters is also visualized in

VERBERNE ET AL. 13 of 23

21699011, 2023, 7, Downloaded from https://agupubs.onlinelibrary.wiley.com/doi/10.1029/2022/P007031 by Cochrane Netherlands, Wiley Online Library on [03/07/2023]. See the Terms and Conditions (https://onlinelibrary.wiley

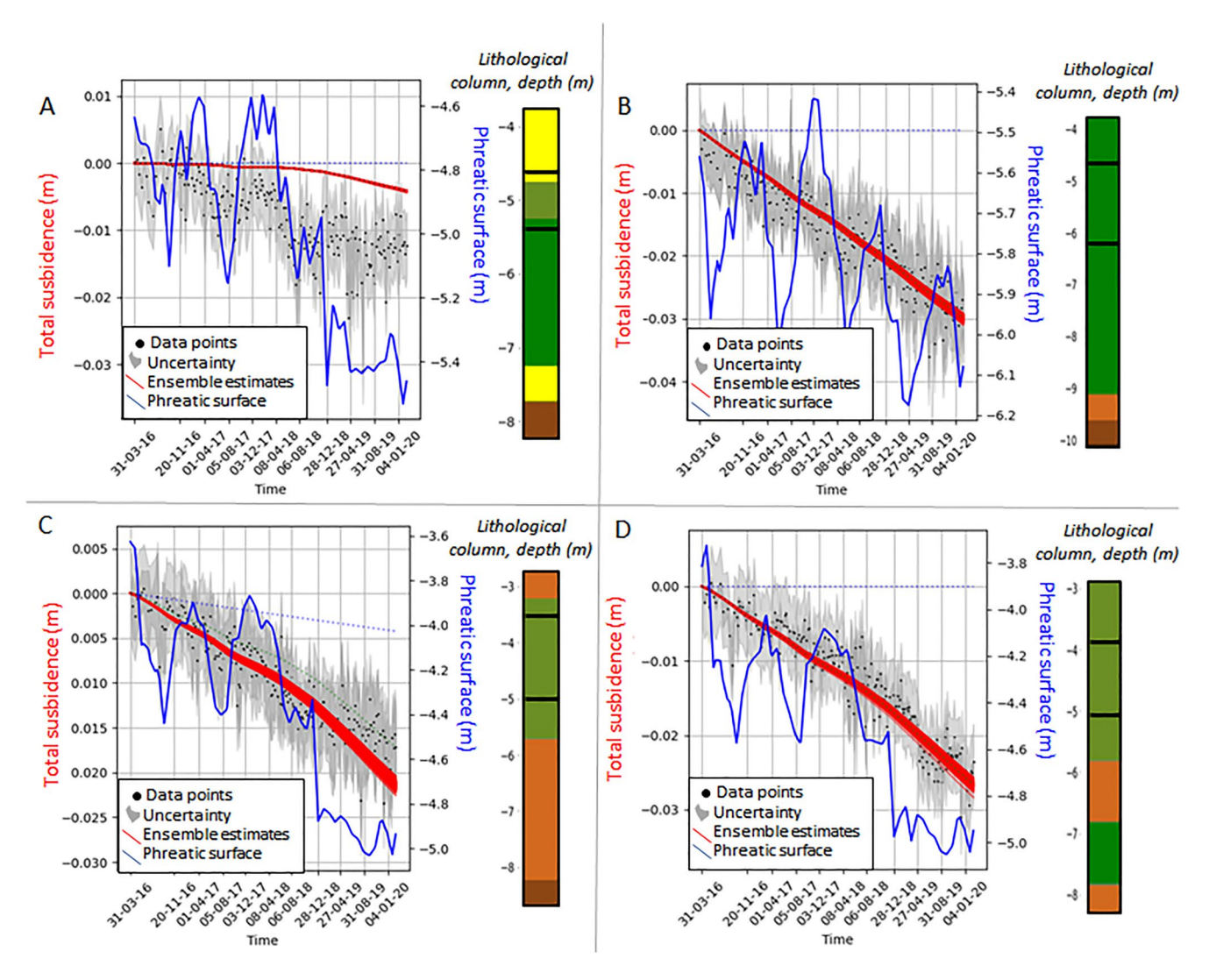


Figure 6. Comparison of surface movements, groundwater levels, and lithology for four example locations. Their locations are indicated in Figure 1b. All figures show the Interferometric Synthetic Aperture Radar-derived surface movements (black points) on the scale of the left y-axis. The uncertainty around them is depicted in gray. It was determined as described in Section 2.1. The red lines are the 200 ensemble members of the optimized fit after four assimilation steps, also on the scale of the left y-axis. The groundwater is the blue line and is with respect to the right y-axis. Next to the graph, a stratigraphic column for that specific location is given, according to the lithoclasses model. The legend of the column is the same as for Figure 4. The black lines note the maximum and minimum phreatic surface level for the simulation period with respect to the lithological column. All y-axes are in meters with respect to NAP. (a) Descending track. This location shows an increase in subsidence rate once the phreatic surface is below the sandy layers, which happens from spring 2018 onwards. (b) Ascending track. Shows the fit of subsidence, where the phreatic surface steadily drops under a seasonal trend. There was no significant increase in the subsidence rate. (c) Descending track. Combination of subsidence due to peat and clay. Enhanced subsidence rate from spring/summer 2018 onwards.

Figure 7. Clay and sandy clay show similar behavior; the behavior of peat is distinctly different. However, the uncertainty for the estimated parameter values for peat is larger than for clay and sandy clay.

A few of the parameters are plotted against each other in Figure 8. For each assimilation step, the 200 estimates of the parameters are plotted against each other. The figure indicates the ensemble spread in the prior estimates and the operation of the smoother by molding the cloud of parameter values. A clear relationship between different parameters evolves, along the lines of the argument in the previous paragraph: different combinations of the shrinkage and oxidation rate and the associated residual height give identical outcomes, as long as they follow the relationship $R = 1 - \frac{C}{v}$. The final ensembles have been fitted to this relationship, as indicated with the dotted black line. The resulting constant C is given in the figure description.

VERBERNE ET AL. 14 of 23

21699011, 2023, 7, Downlo

on Wiley Online Library for rules of use; OA articles are governed by the applicable Creative

Table 2The Parameters That Are Optimized in This Study for All the Locations at the Same Time

Parameter	Pre	Post (ascending)	Post (descending)
V_{sh} clay	0.02 ± 0.005	0.017 ± 0.0012	0.018 ± 0.001
R_h clay	0.60 ± 0.05	0.79 ± 0.017	0.78 ± 0.019
V_{sh} sandy clay	0.02 ± 0.005	0.017 ± 0.0015	0.018 ± 0.0016
R_h sandy clay	0.60 ± 0.05	0.77 ± 0.02	0.77 ± 0.025
V_{ox} Peat	0.01 ± 0.005	0.009 ± 0.003	0.02 ± 0.007
R_h peat	0.90 ± 0.05	0.89 ± 0.04	0.88 ± 0.04

Note. The optimized fit of the ascending and descending track is the result of separate data assimilation procedures, but the results are similar. The pre parameters were chosen based on the study of Fokker et al. (2019). The chi-square error of the ascending track data set has been reduced from 5.2 (prior) to 1.01 (posterior); for the descending track data set it has been reduced from 3.6 (prior) is 3.6 to 0.77 (posterior).

In summary, Table 3 provides an overview of the average contribution to subsidence in mm for the different lithologies for both the ascending and descending satellite tracks.

4. Discussion

4.1. Future Estimates and Spatial Pattern of Subsidence

This study has demonstrated the possibility to make reliable estimates of subsidence related to phreatic groundwater level changes and lithoclass layering. The study area was the urbanized Almere area of the reclaimed South Flevoland polder. For relatively short timescales (years), this enables making estimates of future subsidence, providing indications to drivers and hence tools for designing mitigation strategies. To provide information on expected future subsidence rates, four scenarios for the next 10 years were simulated. The first and fourth scenarios function as a boundary of the influence on subsidence rates by artificially changing phreatic water levels. The first scenario, the most extreme scenario, was to continue the average rate of phreatic groundwater level change toward the future (red in Figure 9b). This is not a realistic assumption: anthropogenic interference on the groundwater

levels would prevent such substantial decrease because of its impact on nature and farming. Scenarios 2 and 3 provide an indication of the magnitude of shrinkage and oxidation, for more realistic conditions. The second scenario was to fix the level at the average height from April 2018 until the end of the research period (blue in Figure 9b)—no more lowering was allowed. This is called water level indexation and is applied in several other polders in the Netherlands as well to reduce subsidence processes. The third scenario fixed the phreatic groundwater level at the average height of the phreatic surface for the research period until April 2018 (green in Figure 9b): the phreatic level was brought back to higher values. The last scenario, finally, increased the water level even further by adding to the third scenario extra 20 cm. This scenario results in phreatic water levels close to the actual surface, where seasonal effects could influence the drainage during periods of increased rainfall, potentially gradually inundating the area. Such a scenario is only realistic for areas which are transformed into nature or used for wet agriculture, which is not the case here. No seasonal trends were added to the scenarios; it is a mere indication of phreatic groundwater level elevation effects on subsidence until 2030.

Figure 9a shows the spatial distribution of the total absolute increase in subsidence since the start of the study related to the different scenarios. The difference between a continuous decrease versus the average level before March 2018 +0.5 m can be up to five cm in 10 years. The spatial plotting also makes it apparent that most of the subsidence is expected in the southwest and northeast of the city of Almere. The area in the northeast part coincides with the course of the Eem paleovalley (Figure 1), where the thickest Holocene sequence is present. Naturally, as this study does not provide a continuous image of subsidence, local alternating Holocene sequences are

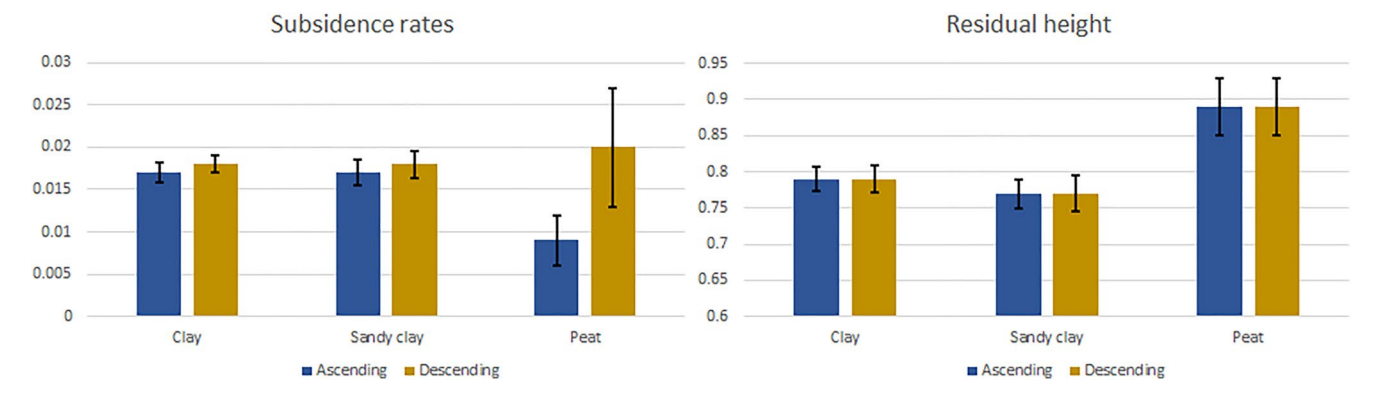


Figure 7. The estimated values of the optimized parameters for subsidence rate and residual height from Table 2 visualized. The outcome of the ascending and descending track is comparable. Clay and sandy clay show similar behavior and peat shows a distinct different behavior, for both the subsidence rates of oxidation and shrinkage and the residual height. The uncertainty of the estimated parameters for peat is larger than for clay and sandy clay.

VERBERNE ET AL. 15 of 23

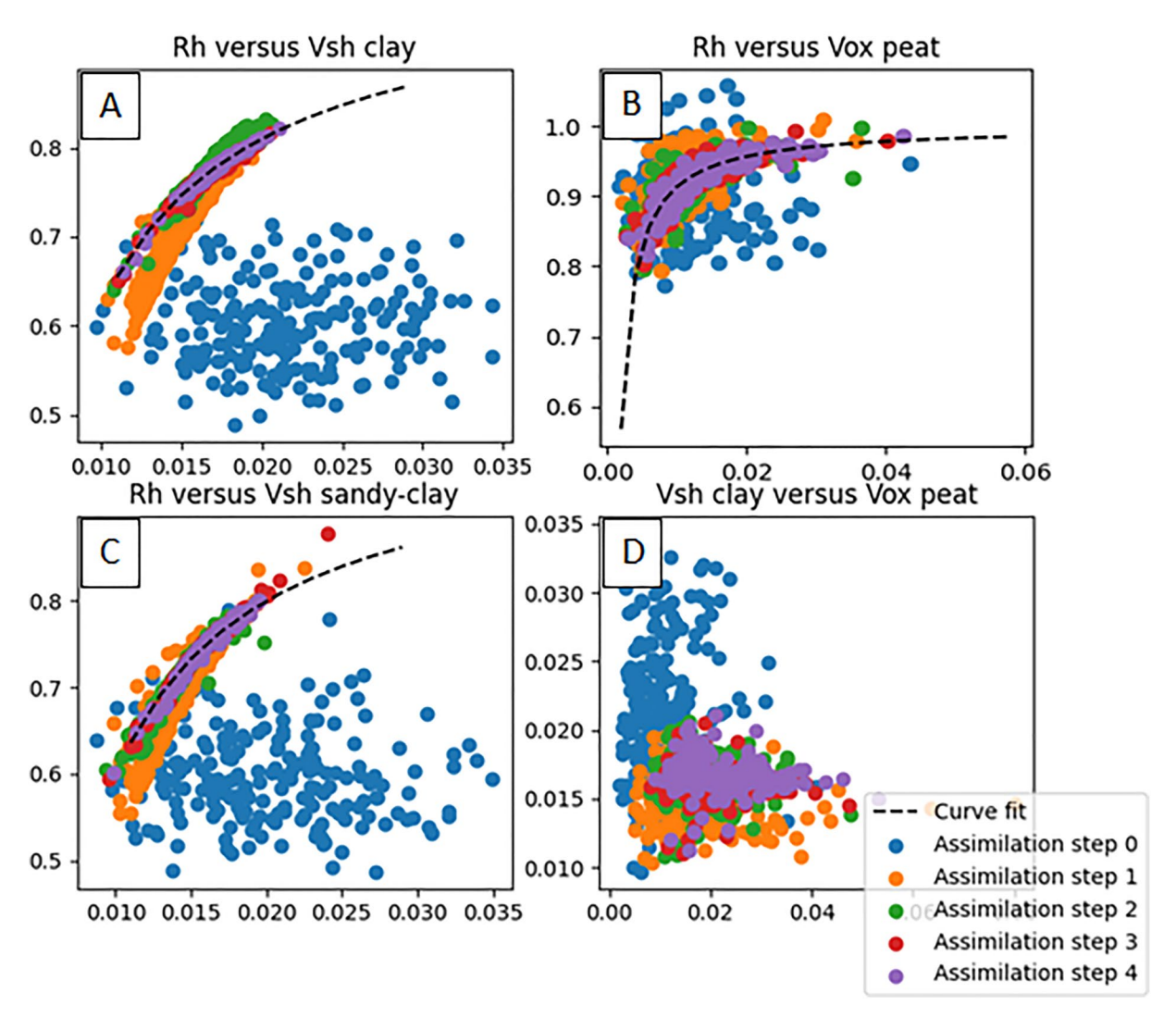


Figure 8. Several of the optimized parameters are plotted against each other for the pre-scenario (assimilation step 0) until the optimized result for the parameters (assimilation step 4) for the ascending satellite track. (a) The residual height of clay versus the shrinkage rate of clay, (b) the residual height of peat versus the oxidation rate of peat, (c) the residual height of sandy-clay versus the shrinkage rate of sandy-clay, (d) the shrinkage rate of clay versus the oxidation rate of peat. There is a strong correlation between the residual height (Rh) and the rate of subsidence (V) within each lithoclass (a–c). There is no clear correlation between the different lithoclasses, as indicated in Figure 6d. For all the lithoclasses, the relation C = v(1 - R) is fitted to the results of assimilation step 4, using an automated least squares polynomial fit. The constants for the line in panel (a) are C = v(1 - R) = 0.0038 yr⁻¹; for (b) it is C = v(1 - R) = 0.0021 yr⁻¹; and for (c) it is C = v(1 - R) = 0.0040 yr⁻¹. (d) Plots two subsidence rates against each other for interlithoclasses correlations, it therefore does not visualize the relationship between residual height and subsidence rate of a specific lithoclass and no curve fit was calculated.

Table 3
The Average Contribution of Clay Shrinkage Versus Peat Oxidation for All the Locations Is Provided Below, in mm/yr

	Ascending	Descending
Average contribution clay shrinkage (mm/yrr)	5.7 ± 2.0	5.8 ± 2.3
Average contribution peat oxidation (mm/yrr)	0.07 ± 0.17	0.20 ± 0.42

Note. Clay incorporates both clay and sandy clay lithoclasses from the lithological model.

not accounted for. The spatial relation of subsidence with Holocene thickness or groundwater level is not a straightforward relation, where clay thickness or groundwater level alone determines the subsidence rate. Our results show that not one single factor influences the spatial pattern of subsidence. This amplifies our need for subsidence modeling on the urban scale.

Figure 9b provides subsidence predictions for the four scenarios for one location. The phreatic groundwater level is a key factor in the subsidence rates. However, even when the phreatic water level is kept constant or is increased, shrinkage and oxidation in the unsaturated zone will continue. From our analysis, it follows that 1 m drop in the phreatic surface will lead to 1 cm of additional subsidence in 5 years. This relationship can help in decisions

VERBERNE ET AL. 16 of 23

21699011, 2023, 7, Dowloaded from https://agupubs.onlinelibrary.wiley.com/doi/10.1029/2022JP007031 by Cochrane Netherlands, Wiley Online Library on [03/07/2023]. See the Terms and Conditions (https://onlinelibrary.wiley.com/doi/10.1029/2022JP007031 by Cochrane Netherlands, Wiley Online Library on [03/07/2023]. See the Terms and Conditions (https://onlinelibrary.wiley.com/doi/10.1029/2022JP007031 by Cochrane Netherlands, Wiley Online Library on [03/07/2023]. See the Terms and Conditions (https://onlinelibrary.wiley.com/doi/10.1029/2022JP007031 by Cochrane Netherlands, Wiley Online Library on [03/07/2023]. See the Terms and Conditions (https://onlinelibrary.wiley.com/doi/10.1029/2022JP007031 by Cochrane Netherlands, Wiley Online Library on [03/07/2023]. See the Terms and Conditions (https://onlinelibrary.wiley.com/doi/10.1029/2022JP007031 by Cochrane Netherlands, Wiley Online Library on [03/07/2023]. See the Terms and Conditions (https://onlinelibrary.wiley.com/doi/10.1029/2022JP007031 by Cochrane Netherlands, Wiley Online Library on [03/07/2023]. See the Terms and Conditions (https://onlinelibrary.wiley.com/doi/10.1029/2022JP007031 by Cochrane Netherlands, Wiley Online Library on [03/07/2023]. See the Terms and Conditions (https://onlinelibrary.wiley.com/doi/10.1029/2022JP007031 by Cochrane Netherlands (https://onlinelibrary.wiley.com/doi/10.1029/2022JP007031 by Cochra

and-conditions) on Wiley Online Library for rule

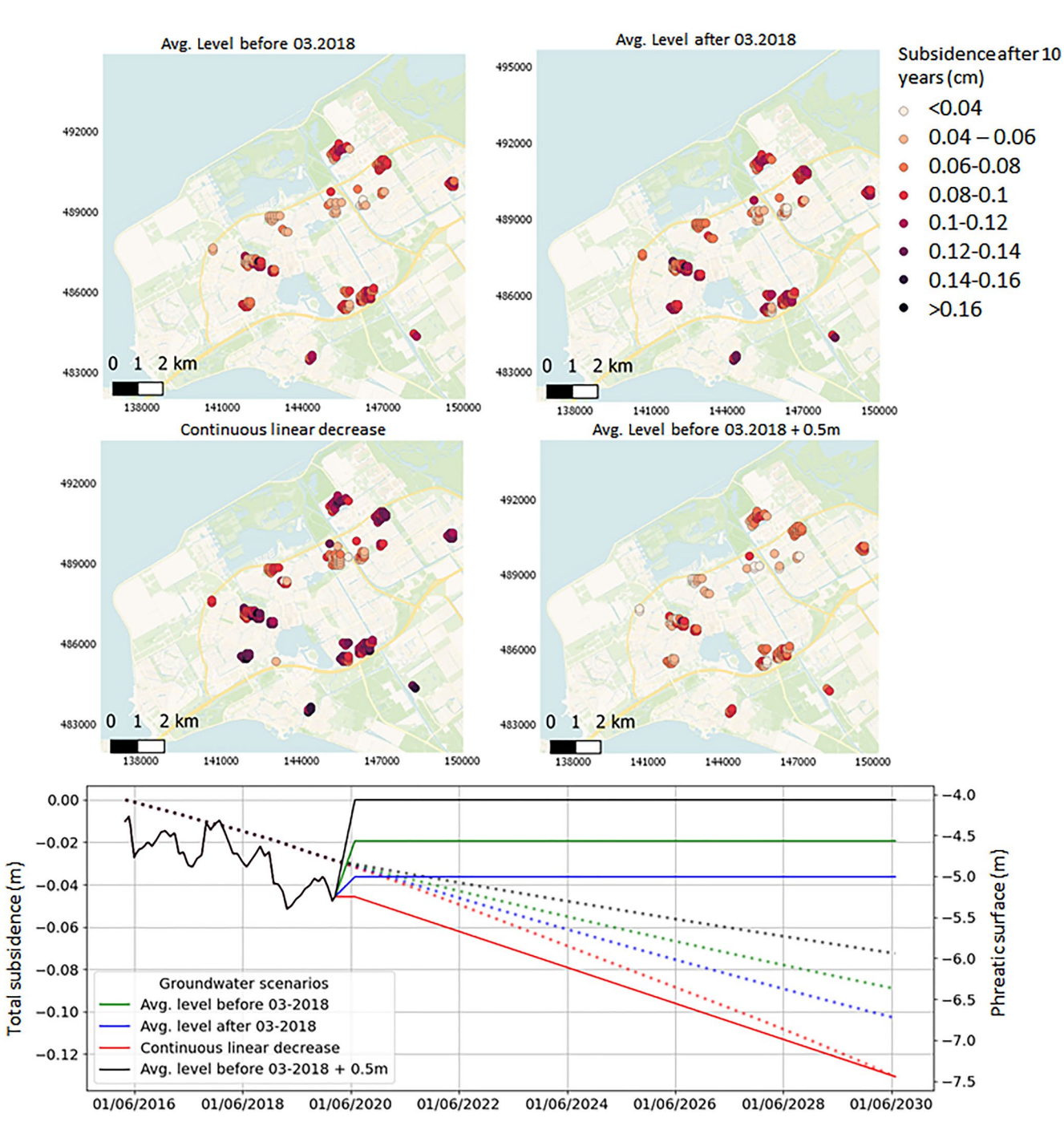


Figure 9. Future estimates of subsidence. (a) Plots the expected subsidence since the start of the study for different scenarios of groundwater development. The scenarios range from largest to smallest drop in the phreatic surface, and hence largest to smallest expected subsidence. Locations are the same as in Figure 1. (b) Shows the subsidence development of one individual location over time, from the start of the study period until 10 years after the end of the study period. The continuous lines show the phreatic surface on the right y-axis, the dashed line shows the modeled subsidence on the left y-axis. In red, the continuous decrease of subsidence is modeled, in blue the average groundwater level from March 2018 until the end of the study period, the green line the average groundwater level of the study period until March 2018 and the black line is the green groundwater level plus 0.2 m.

VERBERNE ET AL. 17 of 23

concerning groundwater management, the single key factor of human influence on the subsidence rate. The results of this study can be used to support science-based mitigation measures.

4.2. Comparison to Other Subsidence Regions

The Flevoland Polder is unique in the Netherlands in the sense that subsidence is dominated by shrinkage of clay. However, clay - dominated subsidence is observed in many other regions in the world (Voosen, 2019). An example is the northern Nile Delta plain in Egypt, where Holocene clay related subsidence is enhanced by climate change that affects the Nile's flow regime (Stanley & Clemente, 2014). There, subsidence ranges from 3.7 to 8.4 mm/yr, which are comparable to the subsidence by clay derived in this study for the South-Flevoland polder.

In and around Venice, Italy, there is ongoing subsidence caused by compression of the natural lagoon (0.0–0.5 mm/yr). More recently, this is aggravated by human-induced subsidence (>2.5 mm/yr) due to ground-water withdrawals (Tosi et al., 2013). Parallels with the South Flevoland polder can be found in the reducing natural consolidation over time and significant subsidence induced by groundwater withdrawals. Both areas must deal with irreversible land lowering caused by groundwater withdrawals, which are required to prevent the area from flooding.

The same comparison can be made with south-east England, where drought is demonstrated to increase subsidence by shrinkage of clay. There, a connection of temperature and precipitation with shrinkage and swelling was made (A. M. Harrison et al., 2012; Pritchard et al., 2015). No estimate of the quantity of subsidence was provided in these papers; however, a link between drought and increased subsidence by shrinkage of clay is also something we identify in the Flevoland Polder.

Despite the differences between these areas in rates of subsidence due to clay shrinkage, the common thread is that all areas are affected by groundwater lowering, either by climate change or anthropogenic causes. Understanding the importance of groundwater level changes to subsidence is therefore of major importance for all these coastal regions across the world. The method presented in this study, and the results in relation to clay behavior of the reclaimed land and the response to groundwater lowering can be of help to tackle this problem.

4.3. Subsidence by Drought

In the results, a slight acceleration of subsidence around summer 2018 is visible. This acceleration is related to relative deep lowering of the phreatic groundwater level. At some locations, this acceleration is more profound than in others, as this is influenced by lithoclass and fluctuations of the phreatic levels as well. As shown in Figure 6, this relative low elevation of the phreatic groundwater level influences the processes responsible for subsidence. Namely, due to a lowered groundwater level, deep peat layers are temporarily aerated, resulting in oxidation and volumetric loss. Furthermore, a deeply lowered phreatic groundwater level can therefore instigate subsidence at locations that were previously not subsiding.

This temporary deeply lowered phreatic groundwater levels are the results of climate change-related drought events, such as the summers of 2018 and 2019 (Hari et al., 2020). Observed accelerated subsidence due to drought is new in the context of the Netherlands. Studies in other (Northwestern) European countries have recently linked drought to increased shrinkage in clay and associated damage to the built environment (e.g., Charpentier et al., 2021). With global warming resulting in more frequent droughts, establishing these relationships becomes increasingly more important.

The results for the effects of drought in this study, however, must be viewed with care. As the number of ground-water datapoints decreases with time, the uncertainty increases. Our results are indicators of drought having an effect, but more extensive and consistent measuring of the phreatic groundwater level is essential to assess groundwater-related subsidence. Especially, the effect of drought on the phreatic groundwater level height is an important link for future scenarios of subsidence and mitigation strategies.

4.4. Implications

Current governmental attention in the Netherlands for shallow subsidence is predominantly focusing on peat oxidation (Van Nieuwenhuizen Wijbenga, 2019). Therefore, the current study fills a gap in the Netherlands

VERBERNE ET AL. 18 of 23

knowledge base. Quantifying the process of clay-driven subsidence is important for optimal decision making regarding shallow subsidence in Almere. Additionally, showing that drought enhances subsidence rates is important for focusing future measures to mitigate subsidence, and connects the problem to climate change. Furthermore, phreatic surface lowering exposing deeper peat beds also increases carbon dioxide emissions by peat oxidation (e.g., Koster et al., 2020).

This study would not have been possible without a structure of nationwide freely available data on the construction of buildings, relative elevation measurements, geology, and groundwater. Still, more data will support to corroborate our findings. Investments in a network to monitor phreatic groundwater level changes and shallow extensometers able to measure volumetric loss within the Holocene sequence are critical herein (cf. Van Asselen et al., 2020). For improved processing of geodetic data, a network of corner reflectors is required to measure surface movement of the ground level (e.g., Yu et al., 2013). Such investments should be conducted in close collaboration with policy makers and spatial planners.

4.5. A Comparison of Parameters With Previous Studies

The South Flevoland polder is unique in the Netherlands with respect to the progressively increasing number of clay and peat beds that encounter contact with atmosphere for the first time since their formation. The estimated subsidence rates are therefore not directly comparable to other polder areas in the Netherlands that have been reclaimed centuries ago.

Earlier studies on subsidence in the South Flevoland polder determined the rates of subsidence due to shrinkage after reclamation estimated based on a few measurements of non-urbanized locations across the South Flevoland polder (De Lange, 2015; De Lange et al., 2012; Fokker et al., 2019). The estimated subsidence in those regions was larger than what we have observed here in the urbanized areas. A reasonable explanation would be that construction has an inhibitory effect on the shrinkage of clay (and when applicable oxidation of organic material) (De Lange, 2015). This study focuses on an urbanized area to estimate the contribution of the different background subsidence processes in urbanized settings.

The residual height estimated by Fokker et al. (2019) lies between 0.50 and 0.67 for clay. However, as mentioned before, the start of modeling subsidence is ~50 years after reclamation in our study, whereas Fokker et al. (2019) start modeling from reclamation onwards; hence, the layers still have their original thicknesses. The values found in this study are higher; ~0.78. Due to the length of the modeling period, only a relation between residual height and reduction rate could be established (Figure 8). A higher residual height can be explained when layers already have partly undergone shrinkage before the start of the observations. Indeed, in our study, the reference is not at the start of exposure to air but a long time later in the compaction history.

A good match between the estimated parameters and the InSAR time series was found for our spatiotemporal model of subsidence in the city of Almere, quantified with the calculated chi-square error, whilst incorporating groundwater levels, lithology, and the physical models. In line with literature, the shrinkage rates of clay are larger than the oxidation rates of peat (Fokker et al., 2019; Schothorst et al., 1982).

The same value for uncertainty is currently attributed to each InSAR-derived data point in space and time. There was no covariance matrix available for the data set. Accurate covariance matrices could increase our ability to fit parameters and models to the data by reducing the weight given to less reliable data points and incorporating interdependencies.

4.6. Correlations Between Parameters

We found correlations between the residual height and reduction rate parameters for the same soil types. This correlation could have been expected from the form of their presence in the forward model. The relationship, as shown in Figure 8, helps in future subsidence estimates. By parameterizing the average behavior of the three lithological types, prediction on future behavior with respect to phreatic groundwater changes can be made even when the individual values of the parameters are rather uncertain.

There is no correlation between the shrinkage rate of clay and the oxidation rate of peat (Figure 8) because lithoclasses act independently. Clay and sandy clay show similar behavior (Figure 8 and Table 2). In the South

VERBERNE ET AL. 19 of 23



Journal of Geophysical Research: Earth Surface

10.1029/2022JF007031

Flevoland polder, sandy clay is the product of tidal dynamics and consists of mm-thick alternating clay and sand beds. The comparable behavior between these thin-bedded sandy-clay and clay deposits indicates the dominance of clay shrinkage within the sandy-clay beds. Apparently, the presence of sand is only minimally preventing these deposits from volumetric loss by shrinkage.

Figure 6a shows a scenario in which the average phreatic groundwater level is located within the uppermost sand bed. Here, the model underestimated observed subsidence. We think the mismatch is related to short drought events not captured by our monthly updated groundwater model. Phreatic groundwater levels that are temporally lowered result in shrinkage of clay directly underneath the upper sand bed, resulting in enhanced subsidence. This explanation is corroborated by the increase in subsidence rate in Figure 6a that coincides with the phreatic surface drop into the clay layer.

5. Conclusions

We have presented a novel data processing and data assimilation workflow with an unprecedented data set to identify processes resulting in anthropogenically induced subsidence around the city of Almere in the reclaimed South Flevoland polder in the Netherlands. The workflow integrates lithoclasses, phreatic groundwater level changes, and InSAR data, with information on construction dates of structures, and a suite of physical models. The assimilation exercise has enabled us to quantify the drivers of subsidence.

Our results have revealed that the shrinkage of shallow clay beds induced by artificial lowering of phreatic groundwater levels is the dominant subsidence process in the South Flevoland polder, with rates up to 6 mm/yr. In line with previous research in the South Flevoland polder, the subsidence rates due to clay shrinkage are significantly higher than those due to peat oxidation, which are up to 0.2 mm/yr. The rates depend critically on the development of phreatic water levels—drought has therefore been identified in this study as an important catalyzer of subsidence. At longer timescales, we estimated that 1 m drop in groundwater level results in 10 millimeter of subsidence in the urbanized area of Almere.

Groundwater governance is the single human activity influencing land subsidence in Almere. Our study high-lights the necessity of high-quality data in order to make trustworthy analyses of subsidence processes and support such governance. Data are obtained by measuring campaigns and continuous monitoring. This includes lithology, groundwater development, and phreatic groundwater level changes. Robust analyses of subsidence processes and quality predictions are possible through the application of an approach that integrates all available data with knowledge on physical processes in a dedicated data assimilation procedure.

Data Availability Statement

Data from the Geological Survey of the Netherlands (TNO-GSN, 2022) was used to construct the lithoclass and groundwater model. The ID codes of the wells used for the groundwater models are given in Data Set S1. Kadaster (2022) was used to verify the age of the buildings. From Rijkswaterstaat (2022) InSAR data products were retrieved. The data points used as input for the ES-MDA procedure for both satellite tracks are included in the Data Sets S2 and S3. Figures were made with Matplotlib v.3.4.3 available under the matplotlib license at https://matplotlib.org and QGIS v3.24 (QGIS Development team, 2022). The Python (Python Software Soundation, 2023) code is available upon request. The data needed to reproduce the results are provided as Data Sets S1, S2, and S3.

${\bf Acknowledgments}$

We are grateful to Joana Esteves-Martins for providing aid with the InSAR data set for this study. We thank our reviewers for their useful and constructive comments. The research presented in this paper is part of the project Living on Soft Soils: subsidence and society (Grant NWA.1160.18.259). This project is funded through the Dutch Research Council (NWO-NWA-ORC), Utrecht University, Wageningen University, Delft University of Technology, Ministry of Infrastructure and Water Management, Ministry of the Interior and Kingdom Relations, Deltares, Wageningen Environmental Research, TNO-Geological Survey of The Netherlands, STOWA, Water Authority: Hoogheemraadschap de Stichtse Rijnlanden, Water Authority: Drents Overiisselse Delta, Province of Utrecht, Province of Zuid-Holland, Municipality of Gouda, Platform Soft Soil, Sweco, Tauw BV, NAM.

References

Allison, M., Yuill, B., Törnqvist, T., Amelung, F., Dixon, T. H., Erkens, G., et al. (2016). Global risks and research priorities for coastal subsidence. Eos, 97, 22–27. https://doi.org/10.1029/2016E0055013

Barbour, E. J., Adnan, M. S. G., Borgomeo, E., Paprocki, K., Shah Alam Khan, M., Salehin, M., & Hall, J. W. (2022). The unequal distribution of water risks and adaptation benefits in coastal Bangladesh. *Nature Sustainability*, 5(4), 295–302. https://doi.org/10.1038/s41893-021-00846-9Barciela Rial, M. (2019). Consolidation and drying of slurries: A building with nature study for the Marker Wadden (Doctoral dissertation). TU Delft. https://doi.org/10.4233/uuid:ae11c3e7-86f2-4c6a-8d53-ee8781d56a72

Barciela-Rial, M., van Paassen, L. A., Griffioen, J., van Kessel, T., & Winterwerp, J. C. (2020). The effect of solid-phase composition on the drying behavior of Markermeer sediment. *Vadose Zone Journal*, 19(1), e20028. https://doi.org/10.1002/vzj2.20028

VERBERNE ET AL. 20 of 23



Journal of Geophysical Research: Earth Surface

- 10.1029/2022JF007031
- Beets, D., & Van der Spek, A. (2000). The Holocene evolution of the barrier and the back-barrier basins of Belgium and The Netherlands as a function of late Weichselian morphology, relative sea-level rise and sediment supply. *Netherlands Journal of Geosciences Geologie En Mijnbouw*, 79(1), 3–16. https://doi.org/10.1017/S0016774600021533
- Bronswijk, J. J. B., & Evers-Vermeer, J. J. (1990). Shrinkage of Dutch clay soil aggregates. *Netherlands Journal of Agricultural Science*, 38(2), 175–194. https://doi.org/10.18174/njas.v38i2.16603
- Burnol, A., Foumelis, M., Gourdier, S., Deparis, J., & Raucoules, D. (2021). Monitoring of expansive clays over drought-rewetting cycles using satellite remote sensing. *Atmosphere*, 12(10), 1262. https://doi.org/10.3390/atmos12101262
- Caló, F., Notti, D., Galve, J. P., Abdikan, S., Görüm, T., Pepe, A., & Balik Şanli, F. (2017). DInSAR-based detection of land subsidence and correlation with groundwater depletion in Konya Plain, Turkey. *Remote Sensing*, 9(1), 83. https://doi.org/10.3390/rs9010083
- Campello, R. J. G. B., Moulavi, D., & Sander, J. (2013). Density-based clustering based on hierarchical density estimates. In Conference: Pacific-Asia conference on Knowledge Discovery and Data Mining (pp. 160–172). https://doi.org/10.1007/978-3-642-37456-2_14
- Candela, T., Chitu, C. G., Peters, E., Pluymaekers, M., Hegen, D., Koster, K., & Peter, A. F. (2022). Subsidence induced by gas extraction: A data assimilation framework to constrain the driving rock compaction process at depth. Frontiers in Earth Science, 10, 1–18. https://doi.org/10.3389/feart.2022.713273
- Candela, T., & Koster, K. (2022). The many faces of anthropogenic subsidence. Science, 376(6600), 1381–1382. https://doi.org/10.1126/science.abn3676
- Carton, J. A., & Giese, B. S. (2008). A reanalysis of ocean climate using simple ocean data assimilation (SODA). *Monthly Weather Review*, 136(8), 2999–3017. https://doi.org/10.1175/2007MWR1978.1
- Castellazzi, P., Martel, R., Galloway, D., Longuevergne, L., & Rivera, A. (2016). Assessing groundwater depletion and dynamics using GRACE and InSAR: Potential and limitations. Groundwater, 54(6), 768–780. https://doi.org/10.1111/gwat.12453
- CBS. (2020). Wijk-en buurtkaart 2020 versie 3. Centraal plan bureau voor statestiek. Retrieved from https://www.cbs.nl/nl-nl/dossier/nederland-regionaal/geografische-data/wijk-en-buurtkaart-2020
- Chang, H., Chen, Y., & Zhang, D. (2010). Data assimilation of coupled fluid flow and geomechanics using the ensemble Kalman Filter. SPE Journal, 15(2010), 382–394. https://doi.org/10.2118/118963-PA
- Charpentier, A., James, M. R., & Hani, A. (2021). Predicting drought and subsidence risks in France. Natural Hazards and Earth System Science Discussions, 22(7), 2401–2418. https://doi.org/10.5194/nhess-2021-214
- Chaussard, E., Amelung, F., Abidin, H., & Hong, S. (2013). Sininking cities in Indonesia: ALOS PALSAR detects rapid subsidence due to groundwater and gas extraction. *Remote Sensing of Environment*, 218, 150–161. https://doi.org/10.1016/j.rse.2012.10.015
- Conroy, P., Van Diepen, S. A. N., Van Asselen, S., Erkens, G., Van Leijen, F. J., & Hanssen, R. F. (2022). Probabilistic estimation of InSAR displacement phase guided by contextual information and artificial intelligence. *IEEE Transactions on Geoscience and Remote Sensing*, 60, 1–11. https://doi.org/10.1109/TGRS.2022.3203872
- Costantini, M., Minati, F., Trillo, F., Ferretti, A., Novali, F., Passera, E., et al. (2021). European ground motion service (EGMS). In 2021 IEEE international geoscience and remote sensing symposium IGARSS (pp. 3293–3296). IEEE. https://doi.org/10.1109/IGARSS47720.2021.9553562 CUR. (1992). Construeren met grond CUR Rapport, (Vol. 162, p. 411).
- Declercq, P., Gérard, P., Pirard, E., Walstra, J., & Devleeschouwer, X. (2021). Long-term subsidence monitoring of the alluvial plain of the Scheldt river in Antwerp (Belgium) using radar interferometry. *Remote Sensing*, 12(6), 1160. https://doi.org/10.3390/rs13061160
- De Glopper, R. J. (1969). Shrinkage of subaqueuous sediments of Lake IJssel (The Netherlands) after reclamation. In *Proceedings first international symposium on land subsidence* (pp. 192–201). IAH.
- De Glopper, R. J. (1973). Subsidence after drainage of the deposits in the former Zuyder Zee and in the brackish and marine forelands in The Netherlands (Vol. 50, p. 205). Van Zee tot Land.
- De Glopper, R. J. (1984). Subsidence in the recently reclaimed IJsselmeerpolder "Flevoland". In *Proc. Third international symposium on land subsidence* (pp. 487–496). IAHS.
- De Glopper, R. J., & Ritzema, H. P. (1994). Land subsidence. In *Drainage principles and applications* (Vol. 16, p. 41). ILRI.
- De Lange, G. (2015). Analyse bodemdaling en zetting Almere (pp. 1210761–000). Deltares Rapport.
- De Lange, G., Gunnink, J., Houthuessen, Y., & Muntjewerff, R. (2012). Bodemdalingskaart Flevoland. Grontmij. GM-0042778.
- $Den \, Haan, E. \, (1996). \, A \, compression \, model \, for \, non-brittle \, soft \, clays \, and \, peat. \, \textit{G\'eotechnique}, \, 46(1), \, 1-16. \, https://doi.org/10.1680/geot.1996.46.1.1 \, and \, peat. \, denote \, pea$
- Deutsch, C., & Journel, A. G. (1998). GSLIB Geostatistical software library and user guide (2nd ed.). Oxford University Press.
- Dinar, A., Esteban, E., Calvo, E., Herrera, G., Teatini, P., Tomás, R., et al. (2021). We lose ground: Global assessment of land subsidence impact extent. Science of the Total Environment, 786, 768. https://doi.org/10.1016/j.scitotenv.2021.147415
- Emerick, A., & Reynolds, A. C. (2013). Ensemble smoother with multiple data assimilation. Computational Geosciences, 55, 3–15. https://doi.org/10.1016/j.cageo2012.03.011
- Eslami, S., Hoekstra, P., Nguyen Trung, N., Ahmed Kantoush, S., Van Binh, D., Duc Dung, D., et al. (2019). Tidal amplification and salt intrusion in the Mekong Delta driven by anthropogenic sediment starvation. *Scientific Reports*, 9(1), 18746. https://doi.org/10.1038/s41598-019-55018-9 Evensen, G. (2009). *Data assimilation, the ensemble Kalman filter* (2nd ed.). Springer.
- Evensen, G., Vossepoel, F. C., & Van Leeuwen, P. J. (2022). Data assimilation fundementals, A unified formulation of the state and parameter estimation problem. Springer. https://doi.org/10.1007/978-3-030-96709-3_1
- Fernández Llamas, A., Martínez, D., Hernández, P., Cristóbal, S., Schwaiger, F., Nuñez, J., & Ruiz, J. (2019). Flight data monitoring (FDM) unknown hazards detection during approach phase using clustering techniques and AutoEncoders. In *Conference paper SESAR ISSN* 0770-1268
- Ferretti, A., Monti-Guarnieri, A., Prati, C., & Rocca, F. (2007). InSAR principles: Guidelines for SAR interferometry processing and interpretation. ESA Publications.
- Fokker, P. A., Gunnink, J., Koster, K., & de Lange, G. (2019). Disentangling and parameterizing shallow sources of subsidence: Application to a reclaimed coastal area, Flevoland, The Netherlands. *Journal of Geophysical Research: Earth Surface*, 124(5), 1099–1117. https://doi.org/10.1029/2018jf004975
- Fokker, P. A., Wassing, B., Van Leijen, F. J., Hanssen, R. F., & Nieuwland, D. (2016). Application of an ensemble smoother with multiple data assimilation of the Bergermeer gas field, using PS-InSAR. Geomechanics for Energy and the Environment, 5, 183–187. https://doi. org/10.1016/j.gete.2015.11.003
- Fryksten, J., & Nilfouroushan, F. (2019). Analysis of clay-induced land subsidence in Uppsala City using Sentinel-1 SAR data and precise leveling. Remote Sensing, 11(23), 2764. https://doi.org/10.3390/rs11232764
- Gazzola, L., Ferronato, M., Frigo, M., Carlo, J., Pietro, T., Zoccarato, C., et al. (2021). A novel methodological approach for land subsidence prediction through data assimilation techniques. Computational Geosciences, 25(5), 1731–1750. https://doi.org/10.1007/s10596-021-10062-1

VERBERNE ET AL. 21 of 23

- Ghil, M., & Malanotte-Rizzoli, P. (1991). Data assimilation in meteorology and oceanography. Advances in Geophysics, 33, 141–266. https://doi.org/10.1016/S0065-2687(08)60442-2
- Google. (2023). Retrieved from https://www.google.nl/maps
- Gunnink, J. (2021). Deklaagweerstand flevopolders. TNO report R10844.
- Guo, H., & Jiao, J. J. (2007). Impact of coastal land reclamation on ground water level and the sea water interface. *Groundwater*, 45(3), 362–367. https://doi.org/10.1111/j.1745-6584.2006.00290.x
- Hanssen, R. F. (2001). Radar interferometry: Data interpretation and error analysis (Vol. 2). Springer Science & Business Media.
- Hari, V., Rakovec, O., Markonis, Y., Hanel, M., & Kumar, R. (2020). Increased future occurrences of the exceptional 2018–2019 Central European drought under global warming. *Scientific Reports*, 10(1), 12207. https://doi.org/10.1038/s41598-020-68872-9
- Harrison, A. M., Plim, J. F. M., Harrison, M., Jones, L. D., & Culshaw, M. G. (2012). The relationship between shrink–swell occurrence and climate in south-east England. *Proceedings of the Geologists' Association*, 123(4), 556–575. https://doi.org/10.1016/j.pgeola.2012.05.002
- Harrison, R., Hol, E. A., & De Graef, M. (2019). On the use of 2D moment invariants in the classification of additive manufacturing powder feedstock. *Material Characterization*, 149, 255–263. https://doi.org/10.1016/j.matchar.2019.01.019
- Hoeksema, R. J. (2007). Three stages in the history of land reclamation in The Netherlands. Irrigation and Drainage, 56(S1), S113–S126. https://doi.org/10.1002/ird.340
- Hoogland, F., Roelandse, A. S., de La Loma González, B., Waterloo, M. J., Mooij, P. W., Verhagen, S. A., & Velstra, J. (2020). Investigating the effectiveness of drain infiltration to minimize peat oxidation in agricultural fields in Flevoland, The Netherlands. *Proceedings of the International Association of Hydrological Sciences*, 382, 747–753. https://doi.org/10.5194/piahs-382-747-2020
- Jones, C. E., An, K., Blom, R. G., Kent, J. D., Ivins, E. R., & Bekaert, D. (2016). Anthropogenic and geologic influences on subsidence in the vicinity of New Orleans, Louisiana. *Journal of Geophysical Research: Solid Earth*, 121(5), 3867–3887. https://doi.org/10.1002/2015JB012636
- $Kadaster.\,(2022).\,Basis registratie \,Adressen\,en\,Gebouwen -\,BAG.\,Retrieved\,from\,www.kadaster.nl/zakelijk/registraties/basis registraties/basis r$
- Kahloot, K., & Ekler, P. (2019). Improving t-SNE clustering and visualization. Computer science, Cropus ID: 229360049.
- Kim, D. J., Feyen, J., Vereecken, H., Boels, D., & Bronswijk, J. J. B. (1993). Quantification of physical ripening in an unripe marine clay soil. Geoderma, 58(1-2), 67-77. https://doi.org/10.1016/0016-7061(93)90085-y
- Kooi, H. (2000). Land subsidence due to compaction in the coastal area of The Netherlands: The role of lateral fluid flow and constraints from well-log data. *Global and Planetary Change*, 27(1–4), 207–222. https://doi.org/10.1016/S0921-8181(01)00067-4
- Koster, K., De Lange, G., Harting, R., De Heer, E., & Middelkoop, H. (2018). Characterizing void ratio and compressibility of Holocene peat with CPT for assessing coastal–deltaic subsidence. The Quarterly Journal of Engineering Geology and Hydrogeology, 51(2), 210–218. https://doi.org/10.1144/qjegh2017-120
- Koster, K., Frumau, A., Stafleu, J., Dijkstra, J., Hensen, A., Velzeboer, I., et al. (2020). Greenhouse peat: A model linking CO₂ emissions from subsiding peatlands to changing groundwater levels. *Proceedings of the International Association of Hydrological Sciences*, 382, 609–614. https://doi.org/10.5194/piahs-382-609-2020
- Koster, K., Stafleu, J., & Cohen, K. M. (2017). Generic 3D interpolation of Holocene base-level rise and provision of accommodation space, developed for The Netherlands coastal plain and infilled palaeovalleys. Basin Research. 29(6), 775–797. https://doi.org/10.1111/bre.12202
- Koster, K., Stafleu, J., Cohen, K. M., Stouthamer, E., Busschers, F. S., & Middelkoop, H. (2018). Three-dimensional distribution of organic matter in coastal-deltaic peat: Implications for subsidence and carbon dioxide emissions by human-induced peat oxidation. *Anthropocene*, 22, 1–9. https://doi.org/10.1016/j.ancene.2018.03.001
- Koster, K., Stafleu, J., & Stouthamer, E. (2018). Differential subsidence in the urbanized coastal-deltaic plain of The Netherlands. *Netherlands Journal of Geosciences*, 97(4), 1–13. https://doi.org/10.1017/nje2018.11
- Lambert, J. W. M., Nieal, L., Stoorvogel-van der Horst, S., Verheijen, E., & Woning, M. (2016). Bodemdaling Almere: Consequenties voor gemeentelijke infrastructuur. Rapport Circulair Cities. TO2.
- Li, D., Li, B., Zhang, Y., Fan, C., Xu, H., & Hou, X. (2022). Spatial and temporal characteristics analysis for land subsidence in Shanghai coastal reclamation area using PSInSAR method. Frontiers in Marine Science, 9, 1000523. https://doi.org/10.3389/fmars.2022.1000523
- Li, L., Zhang, M., & Katzenstein, K. (2017). Calibration of a land subsidence model using InSAR data via the ensemble Kalman filter. Ground-water, 55(6), 871–878. https://doi.org/10.1111/gwat.12535
- Maas, M. (2021). Ook Almere worstelt met bodemdaling. Binnenlands bestuur nr. 12.
- Makaske, B., Van Smeerdijk, D., Peeters, H., Mulder, J., & Spek, T. (2003). Relative water-level rise in the Flevo lagoon (The Netherlands), 5300-2000 cal. yr BC: An evaluation of new and existing basal peat time-depth data. *Netherlands Journal of Geosciences*, 82(2), 115–131. https://doi.org/10.1017/S0016774600020680
- Martín-Antón, M., Negro, V., del Campo, J. M., López-Gutiérrez, J. S., & Esteban, M. D. (2016). Review of coastal land reclamation situation in the world. *Journal of Coastal Research, Special Issue*, 75(75), 667–671. https://doi.org/10.2112/SI75-133.1
- Mayoral, J. M., Castañon, E., & Albarran, J. (2017). Regional subsidence effects on seismic soil-structure interaction in soft clay. Soil Dynamics and Earthquake Engineering, 103, 123–140. https://doi.org/10.1016/j.soildvn.2017.09.014
- Menke, U., van Laar, E., & Lenselink, G. (1999). De Geologie en Bodem van Zuidelijk Flevoland. Flevobericht 415.
- Muntendam-Bos, A. G., Kleuskens, M. H. P., Bakr, M., de Lange, G., & Fokker, P. A. (2009). Unraveling shallow causes of subsidence. *Geophysical Research Letters*, 36(10), L10403. https://doi.org/10.1029/2009gl037190
- Navon, I. M. (2009). Data assimilation for numerical weather prediction: A review. In S. K. Park & L. Xu (Eds.), Data assimilation for atmospheric, oceanic and hydrologic applications. Springer. https://doi.org/10.1007/978-3-540-71056-1_2
- Neumann, B., Vafeidis, A. T., Zimmermann, J., & Nicholls, R. J. (2015). Future coastal population growth and exposure to sea-level rise and coastal flooding A global assessment. *PLoS One*, 10(3), e0118571. https://doi.org/10.1371/journal.pone.0118571
- Nusantara, R. W., Hazriani, R., & Suryadi, U. E. (2018). Water-table depth and peat subsidence due to land-use change of peatlands. IOP Conference Series: Earth and Environmental Science, 145, 012090. https://doi.org/10.1088/1755-1315/145/1/012090
- Peduto, D., Giangreco, C., & Venmans, A. A. (2020). Differential settlements affecting transition zones between bridges and road embankments on soft soils: Numerical analysis of maintenance scenarios by multi-source monitoring data assimilation. *Transportation Geotechnics*, 24, 100369. https://doi.org/10.1016/j.trgeo.2020.100369
- Peduto, D., Huber, M., Speranza, G., van Ruijven, J., & Cascini, L. (2017). DInSAR data assimilation for settlement prediction: Case study of a railway embankment in The Netherlands. Canadian Geotechnical Journal, 54(4), 502–517. https://doi.org/10.1139/cgj-2016-0425
- Peeters, J., Busschers, F. S., & Stouthamer, E. (2015). Fluvial evolution of the Rhine during the last interglacial-glacial cycle in the southern North Sea basin: A review and look forward. *Quaternary International*, 357, 176–188. https://doi.org/10.1016/j.quaint.2014.03.024
- Pritchard, O. G., Hallett, S. H., & Farewell, T. S. (2015). Probabilistic soil moisture projections to assess Great Britain's future clay-related subsidence hazard. Climate Change, 133(4), 635–650. https://doi.org/10.1007/s10584-015-1486-z
- Python Software Foundation. (2023). Python language reference, version 3.11. Retrieved from http://www.python.org

VERBERNE ET AL. 22 of 23



Journal of Geophysical Research: Earth Surface

- 10.1029/2022JF007031
- Rijkswaterstaat. (2018). Rewuierement specification techinical Lot 1: Nationwide deformation map. RWS information.
- Rijkswaterstaat. (2022). Dataregister Rijkswaterstaat Bodembeweging InSAR. Retrieved from https://maps.rijkswaterstaat.nl/dataregister/srv/search?protocol=dataset
- Schmidt, C. W. (2015). Delta subsidence: An imminent threat to coastal populations. *Environmental Health Perspectives*, 123(8), A204–A209. https://doi.org/10.1289/ehp.123-A204
- Schothorst, C. J. (1982). Drainage and behavior of peat soils. In H. de Bakker & M. W. van den Berg (Eds.), *Proceedings of the symposium on peat lands below sea level* (Vol. 30, pp. 130–163). ILRI-publication.
- Schultz, E. (1983). From natural to reclaimed land. Water International, 8(2), 55-60. https://doi.org/10.1080/02508068308686007
- Spaan, B. (2015). Buildings. Waag Society. Retrieved from https://code.waag.org/buildings/
- Spikker, M. (2010). Funderen in Almere. Msc. Thesis. TU Delft.
- Stanley, J. D., & Clemente, P. L. (2014). Clay distributions, grain sizes, sediment thickness and compaction rates to interpret subsidence in Egypt's northern Nile delta. *Journal of Coastal Research*, 30(1), 88–101. https://doi.org/10.2112/JCOASTRES-D-13-00146.1
- Steckler, M. S., Oryan, B., Wilson, C. A., Grall, C., Nooner, S. L., Mondal, D. R., et al. (2022). Synthesis of the distribution of subsidence of the lower Ganges-Brahmaputra Delta, Bangladesh. Earth-Science Reviews, 224, 103887. https://doi.org/10.1016/j.earscirev.2021.103887
- Steenbergen, C., Reh, W., Nijhuis, S., & Pouderoijen, M. (2009). The polder atlas of The Netherlands Pantheon of the low lands. THOTH.
- Sun, Q., Jiang, L., Jiang, M., Lin, H., Ma, P., & Wang, H. (2018). Monitoring coastal reclamation subsidence in Hong Kong with distributed scatterer interferometry. *Remote Sensing*, 10(11), 1738. https://doi.org/10.3390/rs10111738
- Syvitski, J., Kettner, A., Overeem, I., Hutton, E., Hannon, M., Brakenridge, R., et al. (2009). Sinking deltas due to human activities. *Nature Geoscience*, 2(10), 681–686. https://doi.org/10.1038/ngeo629
- Tarantola, A. (2005). Inverse problem theory and method for model parameter estimation. SIAM.
- Teatini, P., Ferronato, M., Gambolati, G., & Gonella, M. (2006). Groundwater pumping and land subsidence in the Emilia-Romagna coastland, Italy: Modeling the past occurrence and the future trend. Water Resources Research, 42(1), W01406. https://doi.org/10.1029/2005WR004242
- Thépaut, J. N. (2003). Satellite data assimilation in numerical weather prediction: An overview. In *Proceedings of ECMWF seminar on recent developments in data assimilation for atmosphere and ocean* (pp. 8–12). ECMWF.
- TNO. (2022). REGIS II, hydrogeologisch model (HGM). Basisregistratie Ondergrond (BRO).
- TNO-GSN. (2022). DINOloket. Retrieved from https://www.dinoloket.nl/en/subsurface-data
- Tosi, L., Teatini, P., & Strozzi, T. (2013). Natural versus anthropogenic subsidence of Venice. Scientific Reports, 3(1), 2710. https://doi.org/10.1038/srep02710
- Van Asselen, S., Erkens, G., & de Graaf, F. (2020). Monitoring shallow subsidence in cultivated peatlands. *Proceedings of the International Association of Hydrological Sciences*, 382, 189–194. https://doi.org/10.5194/piahs-382-189-2020
- Van Asselen, S., Erkens, G., Stouthamer, E., Woolderink, H. A. G., Geeraerts, R. E. E., & Hefting, M. M. (2018). The relative contribution of peat compaction and oxidation to subsidence in built-up areas in the Rhine-Meuse delta, The Netherlands. *Science of the Total Environment*, 636, 177–191. https://doi.org/10.1016/j.scitotenv.2018.04.141
- Van Asselen, S., Stouthamer, E., & Van Asch, T. W. J. (2009). Effect of peat compaction on delta evolution: A review on processes, responses, measuring and modeling. *Earth-Science Reviews*, 92–1(1–2), 35–51. https://doi.org/10.1016/j.earscirev.2008.11.001
- Van De Kerkhof, B., Pankratius, V., Chang, L., van Swol, R., & Hanssen, R. F. (2020). Individual scatterer model learning for satellite interferometry. *IEEE Transactions on Geoscience and Remote Sensing*, 58, 58–2. https://doi.org/10.1109/TGRS.2019.2945370
- Van den Akker, J. J. H., Kuikman, P. J., De Vries, F., Hoving, I., Pleijter, M., Hendriks, R. F. A., et al. (2008). Emission of CO₂ from agricultural peat soils in The Netherlands and ways to limit this emission. In C. Farrell & J. Feehan (Eds.), *Proceedings of the 13th international peat congress* (pp. 1–6).
- Van den Biggelaar, D. F. A. M., Kluiving, S. J., Van Balen, R. T., Kasse, C., Troelstra, S. R., & Prins, M. A. (2014). Storms in a lagoon: Flooding history during the last 1200 years derived from geological and historical archives of Schokland (Noordoostpolder, The Netherlands). Netherlands Journal of Geosciences, 93(4), 175–196. https://doi.org/10.1017/njg.2014.14
- Van der Maaten, L., & Hinton, G. (2008). Visualizing Data using t-SNE. Journal of Machine Learning Research, 9, 2579–2605. Retrieved from https://www.jmlr.org/papers/volume9/vandermaaten08a/vandermaaten08a.pdf?fbcl
- Van der Meulen, M., Doornenbal, J., Gunnink, J., Stafleu, J., Schokker, J., Vernes, R., et al. (2013). 3D geology in a 2D country: Perspectives for geological surveying in The Netherlands. Netherlands Journal of Geosciences Geologie En Mijnbouw, 92(4), 217–241. https://doi.org/10.1017/S0016774600000184
- Van der Meulen, M., Maljers, D., Gesssel, S. F., & Gruijters, S. H. L. L. (2007). Clay resources in The Netherlands. Geologie en Mijnbouw, Netherlands Journal of Geosciences, 86(2), 117–130. https://doi.org/10.1017/S001677460002312X
- Van Dooremolen, W. A., van der Scheer, A., & Winkels, H. J. (1996). Waarnemingen en Prognoses van maaiveldsdaling in Flevoland. Flevobericht 388
- Van Hardeveld, H. A., Driessen, P. P. J., Schot, P. P., & Wassen, M. J. (2017). An integrated modelling framework to assess management strategies steering soil subsidence in peatlands. Environmental Impact Assessment Review, 66, 66–77. https://doi.org/10.1016/j.eiar.2017.06.007
- Van Nieuwenhuizen Wijbenga, C. (2019). Rijksbrede inzet op bodemdaling. Ministerie van Infrastructuur en Waterstaat. IENW/BSK-2019/135551.
- Viscchedijk, M. A. T., & Trompille, V. (2009). MSettle Version 8.2. Emankment design and soil settlement prediction. Deltares report.
- Voosen, P. (2019). Seas are rising faster than believed at many river deltas. Science, 441(6426), 441. https://doi.org/10.1126/science.363.6426.441 Vos, P. C. (2015). Origin of the Duthc coastal landscape. Long-term landscape evolution of The Netherlands during the Holocene, described and
- Vos, P. C. (2015). Origin of the Duthc coastal landscape. Long-term landscape evolution of The Netherlands during the Holocene, described and visualized in national, regional and local palaeogeographical map series (Doctoral Dissertation). Utrecht University Repository. Retrieved from https://dspace.library.uu.nl/handle/1874/315553
- Wang, M., Li, T., & Jiang, L. (2016). Monitoring reclaimed land subsidence in Hong Kong with InSAR technique by persistent and distributed scatters. Natural Hazards, 82(1), 531–543. https://doi.org/10.1007/s11069-016-2196-1
- Wang, W., Liu, H., Li, Y., & Su, J. (2014). Development and management of land reclamation in China. Ocean & Coastal Management, 102B, 415–425. https://doi.org/10.1016/j.ocecoaman.2014.03.009
- Wegmüller, U., Santoro, M., Werner, C., & Cartus, O. (2015). On the estimation and interpretation of Sentinel-1 tops InSAR coherence. In *Proc. 'Fringe 2015 workshop'*.
- Yu, B., Liu, G., Li, Z., Zhang, R., Jia, H., Wang, X., & Cai, G. (2013). Subsidence detection by TerraSAR-X interferometry on a network of natural persistent scatterers and artificial corner reflectors. Computers & Geosciences, 58, 126–136. https://doi.org/10.1016/j.cageo.2013.04.020
- Zaadnoordijk, W. J., Bus, S. A. R., Lourens, A., & Berendrecht, W. L. (2018). Automated time series modelling for piezometers in the national database of The Netherlands. *Groundwater*, 57(6), 834–843. https://doi.org/10.1111/gwat.12819

VERBERNE ET AL. 23 of 23